공학석사 학위논문

Development of Interferometer System for Versatile Experiment Spherical Torus (VEST)

VEST 장치를 위한 간섭계 시스템 개발

2012 년 8 월

서울대학교 대학원

에너지시스템공학부

최 다 혜

Development of Interferometer System for Versatile Experiment Spherical Torus (VEST)

지도 교수 황 용 석

이 논문을 공학석사 학위논문으로 제출함
2012 년 8 월

서울대학교 대학원
에너지시스템공학부
최 다 혜

최다혜의 공학석사 학위논문을 인준함
2012 년 8 월

위 원 장 _____ 김 곤 호 (인)

부위원장 _____ 황 용 석 (인)

위 원 _____ 나 용 수 (인)

Abstract

Development of Interferometer System for Versatile Experiment Spherical Torus (VEST)

Da-Hye Choi

Department of Energy System Engineering

The Graduate School

Seoul National University

A microwave interferometer system has been developed to measure plasma densities of Versatile Experiment Spherical Torus (VEST) at Seoul National University. Initial operation of the VEST will focus on double null merging start-up schemes using two partial solenoid coils installed at both vertical ends of a center stack. In order to understand plasma behaviors of this machine, evolution of density profiles is an important plasma parameter to be diagnosed. The interferometer system to measure line-integrated plasma densities at several horizontal planes by moving vertically in repeating identical shots is designed, and a single chord interferometer system in Mach-Zehnder type is constructed and tested as a first step by developing a 94GHz heterodyne microwave system and a relevant beam focusing system.

The interferometer system comprises 94GHz heterodyne microwave system and beam focusing system. The frequency of 94GHz has been chosen in the consideration of cutoff frequency, resolution of measurement, vibration effect and refraction effect. The microwave system injects microwave beams, receives phase-shifted beams, and generates output signals to measure the

plasma density with electronic circuits. Two 94 GHz Gunn Oscillators are used in a heterodyne Mach-Zehnder type configuration. IF frequency is set to about 60MHz, and the phase difference of signals from two mixers will be transmitted to phase comparator, which generates voltage signal in proportion to the phase shift.

According to quasi-optical Gaussian beam path analysis, beam focusing systems which can focus and reflect the beam for effective beam reception and enhanced spatial resolution are designed. A beam focusing system with a pair of plano-convex spherical lenses and a concave spherical mirror is designed for a single chord measurement, and another system with two pairs of plano-convex cylindrical lenses and a concave cylinder mirror is designed for the interferometer system with vertical moving measurement capability.

The design of the beam focusing system and the beam path analysis for the single chord measurement are experimentally verified where an experimental test bed is built with real dimensions of a vacuum vessel. Optimum distances between the optical components and the beam radii along the beam path obtained from the experiments are in good agreements with the beam path analysis using the Gaussian optics. Both experiments and numerical calculations confirm that the designed beam focusing system maximize the spatial resolution of the measurement to the value of 20 mm; moreover, the beam waist is located at the center of the plasma to generate a phase shift more effectively in plasmas.

Based on these preliminary experiments, the horizontal single chord configuration is installed on the upper chamber of the VEST. Component testing has been done to optimize the alignment of the beam focusing system and to test phase shift with a material of known refractive index, of which results show a good agreement with theoretically predicted phase shift value. Also, real plasma measurements in ECH pre-ionization experiment are performed with triple probe measurements. Plasma electron densities are estimated from the measured line-integrated density, showing good agreements with triple probe measurements. The single chord interferometer

system developed in this thesis is expected to be used in the measurements of line integrated plasma densities during the start-up phase of VEST, and a full interferometer system with vertical moving measurement capability will be completed in near future for the measurement of plasma density profiles.

Keywords : Interferometer, VEST, Plasma electron density measurement, Millimeter wave, Gaussian beam, Quasi-optical system

Student Number : 2010-23347

Contents

List of Tables

List of Figures

Chapter 1 Introduction

Plasma diagnostics are of great importance in thermonuclear fusion plasma research. Measuring plasma properties in various space and time scales benefits not only evaluating plasma property itself, but also controlling and optimizing plasma performance in the fusion plasma machine. Requirements for plasma measurements are determined based on operating scenarios and machine specifications, which comprise magnetic measurements, fusion product measurements, and measurements of electron temperatures, electron densities, ion temperatures, impurities, radiated power, and the q-profile [1, 2].

Among them, plasma density is one of the most important quantities characterizing plasma. Especially in thermonuclear fusion research, high-density plasmas are of interest for which several approaches are considered: interferometer, refractometry, Thomson scattering and reflectometry [1-3], utilizing electromagnetic wave of appropriate condition. If the toroidal magnetic is well known, electron density could also be determined from the result of polarimeter, the product of electron density and toroidal magnetic field, thus toroidal interferometer/polarimeter is able to achieve electron density [4, 5]. Probe measurement is also common approach to measure plasma density, yet it has some disadvantages of disturbance of the plasma and erosion of the tip of the probe due to sputtering [6, 7].

Interferometer, however, inherently does not perturb the plasma and allows reliable result, thus it plays a fundamental role in measuring electron density in almost every fusion plasma machine. Two or more waves are allowed to interfere by coherent addition electric fields to determine plasma density, then interferometer compares phase difference between two beams which have taken different optical path. The phase difference is represented

by refractive index, and could be directly represented by plasma density if the wave satisfies the condition of O-wave, in which wave propagates perpendicular to magnetic field and the oscillating electric field is parallel to the magnetic field [8, 9].

1.1 Motivation and objectives

Recently a spherical torus named VEST (Versatile Experiment Spherical Torus) has been designed and constructed at Seoul National University as a low cost, compact, educational fusion research device to investigate emerging scientific and engineering topics such as magnetic reconnection, sequential double null merging, innovative divertors, and non-inductive current drives [10].

The initial operation of VEST will focus on double null merging start-up schemes using two partial solenoid coils installed at both vertical ends of a center stack. These partial solenoid coils provide sufficient magnetic flux without losing low aspect ratio characteristics that make high performance with extremely high beta possible. A very elongated vacuum chamber extended with top and bottom regions is designed to accommodate partial solenoids, which will be advantageous in double null merging start-up. In this condition, vertical movement of plasma has importance in analyzing VEST plasma characteristics.

In order to measure plasma properties of VEST, currently installed diagnostic system comprises 94 GHz heterodyne interferometer system, a monochromator for H-alpha monitoring and 3 Rogowski coils installed outside the vacuum chamber. Also, various magnetic diagnostics such as pick-up coils, flux loops and in-vessel Rogowski coils are under preparation. An internal magnetic probe array using both inductive coils and hall sensors is also under development for the vacuum field measurement and the magnetic field measurement during double null merging start-up. In addition, a 20 kHz

fast CCD camera and a soft X-ray imaging system will be used to monitor plasma evolutions.

Among those diagnostic systems, interferometer is reliable measurement method for plasma electron density, one of the basic plasma properties which should be known fundamentally. Once the interferometer system is developed, the system could directly measure line integrated electron density routinely. However, depending on specific conditions of the plasma device, interferometer system requirements differ significantly. Therefore, specific constraints should be studied in order to develop appropriate interferometer system for the machine.

Also, optimum frequency range should be selected to develop wave launching and receiving electronic systems. For the VEST, relatively low density device as a fusion plasma device, wave of low frequency would be apt than waves for big tokamaks. In this case, refraction effects increase, reducing spatial resolution thus worsen the measurement efficiency, thus it requires beam focusing system to converge diverging beam and enhance measuring efficiency. Since spatial factors affect beam focusing system a lot, a special beam focusing system is necessary for the VEST geometry. In addition, depending on measurement, the beam focusing system configurations should be modified for optimum measurement.

This thesis deals with the developing process of VEST interferometer system, therefore the objectives of this thesis are to:

- Design the interferometer system satisfying requirements given by specifications of the VEST
- Fabricate and optimize the interferometer system to enable measuring plasma density
- Install and test verification on the machine

This requires a clear understanding of engineering constraints of the VEST, thus fundamental analyses will be performed as follows:

- Analyzing frequency constraints for the VEST system in regard to cutoff frequency, refraction effect, system resolution, vibration effect, and fringe jump

- Quasi-optical analysis on Gaussian beam to design beam focusing system by optimizing optical elements; lens and mirror

Also, in developing process, several tests will be taken in order to verify designed system as follows:

- Preliminary experiments with the beam focusing system on a horizontal plane model reflecting a real-sized vacuum vessel, before installation on the VEST machine

- Test for optimizing beam focusing system during the installation

- Test with a material of known refractive index to verify its ability of phase shift

- Test measurement on ECH pre-ionization experiment and comparison of its result with triple probe measurement result

1.2 Thesis outline

In this thesis, developing process for optimum interferometer system on VEST, consists of microwave electronics system and beam focusing system, is explored against some constraints of the VEST.

In chapter 2, previous works on millimeter wave interferometer systems are described as a reference for the VEST millimeter wave interferometer. Also, background theories which are necessary to develop the VEST interferometer system is presented, including theory of interferometery and quasi-optics theory.

In chapter 3, design process for overall VEST interferometer system is explored. According to design requirements which reflect special characteristics of the VEST device, overall system is designed including single chord measurement configuration and vertical moving configuration.

In chapter 4, microwave electronics system in the VEST interferometer system is described. Frequency selection process is discussed to optimize microwave probing beam for the VEST geometry and plasma condition. Also, microwave components of heterodyne interferometer system which generate and mix microwave are presented.

In chapter 5, beam focusing system is developed. With regard to measurement configurations, beam focusing system requirements are discussed. Based on quasi optics theory, optical elements are designed to satisfy the requirements. And for the case of single chord measurement system, which would be utilized as the initial measurement configuration, beam focusing experiment is presented and results are discussed to verify designed system.

In chapter 6, two kinds of test experimental results on VEST are discussed. One verifies installed interferometer system on VEST, whether it works properly as interferometer by measuring line integrated density of test material of known refractive index. The other measures line integrated density

on ECH pre-ionization experiments, and results are discussed comparing with triple probe measurement results

In chapter 7, interferometer development processes of this thesis are summarized and conclusions and future works using this system are presented.

Chapter 2
Literature review and background theory

2.1 Millimeter wave interferometer systems

Plasma densities in the plasma fusion devices have been gradually increased, so that plasma frequencies are in the range of millimeters (wavelength of several millimeters) to submillimeters (wavelength below several millimeters, micrometer range) [11]. Although a fundamental principle of interferometer measurement is identical to both frequency ranges, wave sources are obviously different as laser for submillimeter wave and microwave electronic components for millimeter wave. Since wave frequency used for interferometer is proportional to density of the device, millimeter wave interferometer is used usually for the relatively low density plasma device or for the initial operational phase of the high density device. Therefore the VEST interferometer system is of interest to millimeter wave.

TFTR (Toroidal Fusion Test Reactor) used 1 millimeter wave interferometer for the measurement of line integral electron density [12]. A two-pass interferometer at 285 GHz was developed on the horizontal midplane of the TFTR in order to provide a two-pass line integral electron density measurement, of which line-average density was $2\times10^{20}m^{-3}$. This two-pass design utilized a stainless steel, spherical surfaced, rectangular mirror with a focal length of 200 cm mounted on the inner vacuum vessel wall and the antenna was mounted on a vacuum flange. Thus two-pass beam consisted of initially launched beam and reflected beam. A heterodyne system was designed to allow continuous wave operation, avoid amplitude modulation problem and reduce noise sidebands, instead of homodyne system. This interferometer system allowed to measure density during major radial compression of the plasma, and also gave an input signal to the gas feedback control system. This type of two-pass design will be employed for the VEST,

which benefits reducing power loss through long waveguides.

On the JET (Joint European Torus) experiment, a single channel 2 mm microwave interferometer was developed to measure the line integrated electron density along a single vertical plasma chord [13]. Jet is a large controlled fusion research tokamak with a major radius, R, of 2.96 m and the single chord was located at R=3.14 m. Since the interferometer components should be located outside the biological shield, transmission path was more than 70 m with an oversized waveguide. In order to provide a continuous fringe train on the interferometer output signal in the absence of plasma, a Mach-Zender configuration was used with unequal length plasma and reference paths and sweeping the klystron frequency. An average electron density change along the chord was $\pm 7 \times 10^{15} m^{-3}$ for typical plasma with a 3 m vertical diameter, and the system operated routinely and the maximum JET plasma densities of between 3 and $4 \times 10^{19} m^{-3}$ about that time was measured with high density resolution. Although it utilized millimeter wave, its system size is too large to be employed to the VEST system.

CDX-U (current drive experiment-upgrade) developed a versatile 2 mm (140 GHz) scanning interferometer in order to measure the line integral density profile of both horizontal and vertical views and the Faraday rotation (for plasma currents larger than 10 kA) of the vertical view [14]. The two-dimensional translation table system operates in horizontal and vertical modes. A horizontally scanning mode provides a horizontal view of the plasma by moving a horizontal chord vertically between shots, and a vertically scanning provides a vertical view from a scanned vertical chord by moving the entire system radially. Gaussian Optics Lens Antenna (GOLA), a lens-corrected scalar feed horn antenna, is used for vertical view optics to produce a beam of radiation which is symmetric in both the E and H-planes. Two channel 140 GHz heterodyne receiver was developed for microwave electronics system, with IF frequency of 300 MHz. This system utilized interferometer at various view, thus helps to provide modifying interferometer configurations.

For a commissioning phase of KSTAR (Korea Superconducting Tokamak Advanced Research) where peak electron density of $10^{19} m^{-3}$ and plasma radius of 30 cm are expected, a 280 GHz single channel millimeter wave system was developed on a horizontal line [15, 16]. Because of the cryogenically cooled superconducting coils, a retractable cassette system was installed on a horizontal diagnostics port. The cassette includes beam focusing module which consists of two concave mirrors and two plane mirrors, and this focusing function as enhance the signal-to-noise ratio by increasing the receiving beam power and by minimizing beam width inside the plasma. The microwave beam passes through the plasma following a triangular shape, not a center line, and one of the tiles at inner wall of vacuum vessel was fabricated as a concave mirror to reflect a microwave. IF signal frequency is 60 MHz and the phase resolution of 1/20 fringe could be provided with the multifringe counting capability of up to 16 fringes. The focusing system used in this system could be utilized, but above all, it gives idea of focusing method.

In conclusion, from previous work on millimeter wave interferometer, interferometer methods on millimeter wave could be obtained. However, although refraction effect is significant in this wave range, no precise works on beam focusing have been done except KSTAR. But KSTAR geometry is different to small laboratory devices, other approach on refraction effect on millimeter wave seems to be needed.

2.2 Theory of interferometry

2.2.1 Plasma O-wave and phase shift

Interferometer uses electromagnetic O-wave to measure plasma electron density from phase shift. From this wave theory in this section, dispersion relation which relates wave property with density, then line integrated density could be derived from this relation.

For a typical Tokamak geometry, a large portion of magnetic field consists of which is formed along a toroidal direction. In this case, when we inject electromagnetic wave from outside of the Tokamak, it acts as perpendicular to the toroidal field, B_0. If the perturbed electric field, E_1, is parallel to B_0, the wave is the ordinary wave that is not affected by the magnetic field. The electromagnetic waves with $B_0 = 0$ and $B_1 \neq 0$ - transverse electromagnetic waves- are able to be applied as an assumption [8].

By the procedure of linearization, the dependent variables are separated into an equilibrium part with subscript 0 and a perturbation part with subscript 1: $E = E_0 + E_1$ and $B = B_0 + B_1$. For light waves in a plasma, the relevant Maxwell equations are

$$\nabla \times \mathbf{E_1} = -\dot{\mathbf{B}}_1 \tag{2.1}$$

$$c^2 \nabla \times \mathbf{B}_1 = \frac{\dot{\boldsymbol{j}}_1}{\varepsilon_0} + \dot{\mathbf{E}}_1 \tag{2.2}$$

where c is the speed of light. The time derivative of this and the curl of the result are

$$c^2 \nabla \times \dot{\mathbf{B}}_1 = \frac{1}{\varepsilon_0} \frac{\partial \boldsymbol{j}_1}{\partial t} + \ddot{\mathbf{E}}_1 \tag{2.3}$$

$$\nabla \times (\nabla \times \boldsymbol{E}_1) = \nabla(\nabla \cdot \boldsymbol{E}_1) - \nabla^2 \boldsymbol{E}_1 = -\nabla \times \dot{\boldsymbol{B}}_1 \tag{2.4}$$

Assuming waves as $exp[\,i(kx-wt)\,]$ and eliminating $\nabla\times\dot{\boldsymbol{B}}_1$,

$$-\mathbf{k}(\mathbf{k}\cdot\mathbf{E}_1)+\mathbf{k}^2\mathbf{E}_1=\frac{\mathrm{i}\omega}{\varepsilon_0 c^2}\mathbf{j}_1+\frac{\omega^2}{c^2}\mathbf{E}_1 \tag{2.5}$$

Since the transverse wave has $\mathbf{k}\cdot\mathbf{E}_1=0$,

$$(\omega^2-c^2\boldsymbol{k}^2)\boldsymbol{E}_1=-i\omega\boldsymbol{j}_1/\varepsilon_0 \tag{2.6}$$

When it comes to light waves or microwaves, ions are able to be considered as fixe, the current is represented with electron motions only: $\boldsymbol{j}_1=-n_0e\boldsymbol{v}_{e1}$.

From the linearized electron equation of motion for $kT_e=0$,

$$m\frac{\partial\boldsymbol{v}_{e1}}{\partial t}=-e\boldsymbol{E} \tag{2.7}$$

$$\boldsymbol{v}_{e1}=\frac{e\boldsymbol{E}_1}{im\omega} \tag{2.8}$$

Then equation is represented as

$$(\omega^2-c^2\boldsymbol{k}^2)\boldsymbol{E}_1=\frac{i\omega}{\varepsilon_0}n_0e\frac{e\boldsymbol{E}_1}{im\omega}=\frac{n_0e^2}{\varepsilon_0 m}\boldsymbol{E}_1 \tag{2.9}$$

With the representation of plasma frequency, dispersion relation is,

$$\omega^2=\omega_p^2+c^2\boldsymbol{k}^2 \tag{2.10}$$

From this relation, for a given wave frequency ω, as the plasma density increases, plasma frequency ω_p increases thus propagation constant *k* decreases. At some point *k* becomes zero, then the wave is not available to propagate anymore; cutoff occurs. This density is called as a critical density n_c, which is represented as

$$n_c = m\varepsilon_0\omega^2 / e^2 \tag{2.11}$$

When two waves, probe wave and reference wave, are transmitted through difference materials, phase difference is given by

$$\Delta\phi = \int \left(k_{plasma} - k_0\right) dl = \int \frac{\omega}{c}\left(N - 1\right) dl \tag{2.12}$$

, where N is refractive index, which is given from dispersion relation in the plasma,

$$N^2 = 1 - \frac{\omega_p^2}{\omega^2} = 1 - \frac{n_e e^2}{\varepsilon_0 m}\frac{1}{\omega^2} = 1 - \frac{n_e}{n_c} \tag{2.13}$$

Thus phase shift is

$$\Delta\phi = \frac{\omega}{c}\int\left(\sqrt{1 - \frac{n_e}{n_c}} - 1\right) dl \tag{2.14}$$

If plasma electron density is low enough than cutoff density, phase shift is able to be represented as

$$\Delta\phi = \frac{\omega}{2cn_c}\int n_e dl = 2.82\times10^{-15}\lambda\int n_e dl \tag{2.15}$$

With line average density $\bar{n}_e$, phase shift is

$$\Delta\phi = \frac{\omega}{2cn_c}\bar{n}_e l \tag{2.16}$$

The corresponding fringe number is

$$F = \Delta\phi / 2\pi = 4.49\times10^{-16}\lambda\int n_e dl \tag{2.17}$$

Therefore, from the phase shift of two probing beams, line-integrated

electron density can be measured.

2.2.2 Heterodyne interferometer

In interferometer, two or more waves are allowed to interfere by coherent addition of electric fields. Therefore, observed intensity is modulated depending on whether the fields interfere constructly or destructly, in phase or out of phase [2]. For simple interferometer of two fields $E_1 \exp i\omega t$ and $E_2 \exp i(\omega t + \phi)$ with phase difference ϕ, then the total field becomes

$$E_t = (E_1 + E_2 \exp i\phi) \exp i\omega t \tag{2.18}$$

. And corresponding power detected becomes square of the total field,

$$\left|E_t\right|^2 = \left[E_1^2 + E_2^2\right]\left[1 + \frac{2E_1E_2}{E_1^2 + E_2^2}\cos\phi\right] \tag{2.19}$$

. Therefore, phase shift ϕ is proportional to the output power of the interferometer. However, there are some sources of ambiguity and error to determine plasma density from the output power of the interferometer.

One source of ambiguity is amplitude variations of two fields, E_1 and E_2. According to Equation (2.19), this variation cannot be distinguished from the phase shift. However, this problem can be removed by measuring both E_1 and E_2.together with output power, a bit complex though.

The other source of ambiguity is the phase change direction. Since in Equation (2.19), phase shift is represented as cosine function, thus output power shows periodic signal per π. For example, even if the phase becomes longer than π, it cannot be distinguished from the output power of cosine function since cosine function is symmetric per π. Therefore phase variation

$\Delta\omega = d\phi / dt$, given as positive value, cannot determine whether the change is constructive or destructive as shown in Figure 2.1 (homodyne). However, If one change one of initial frequency slightly, then phase change direction could be determined from Figure 2.1 (heterodyne). Initially given phase difference $\Delta\omega$ corresponds to IF, intermediate frequency of interferometer system.

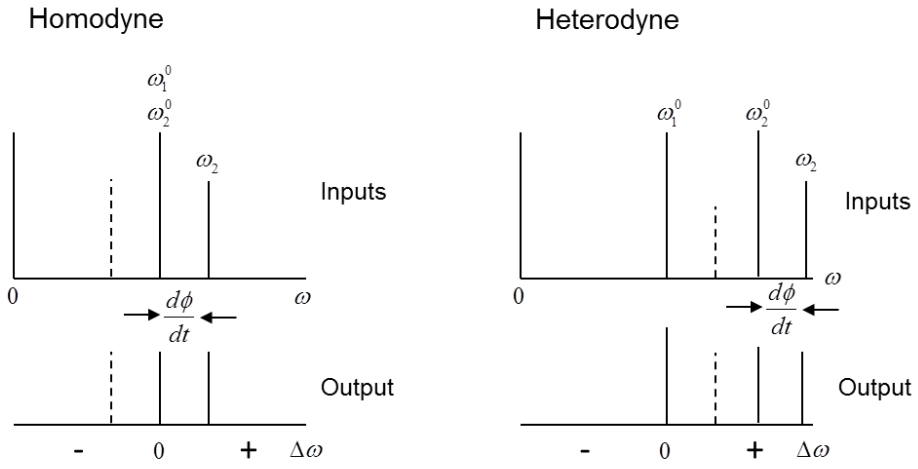

Figure 2.1 Contrary to homodyne system, heterodyne interferometer with IF (intermediate frequency) of $\Delta\omega$ enables to distinguish phase variation [2].

2.2.3 Mach-Zehnder interferometer

Various types of interferometer configuration are used, but main systems are two of them, the Michelson interferometer configuration and the Mach-Zehnder configuration, as shown in Figure 2.2. The Michelson interferometer consists of one beamsplitter, two arms in which the beams travel in both directions, and two outputs, one of which is along the input. Although Mach-Zehnder configuration also corresponds to a two-beam interferometer, the beams travel in only one direction contrary to the Michelson configuration. In both configurations, phase changes are produced by variations of the refractive index N in one arm [2]. The basic difference between two configurations is that beamsplitter is also used to recombine the beams for the Mach-Zehnder configuration.

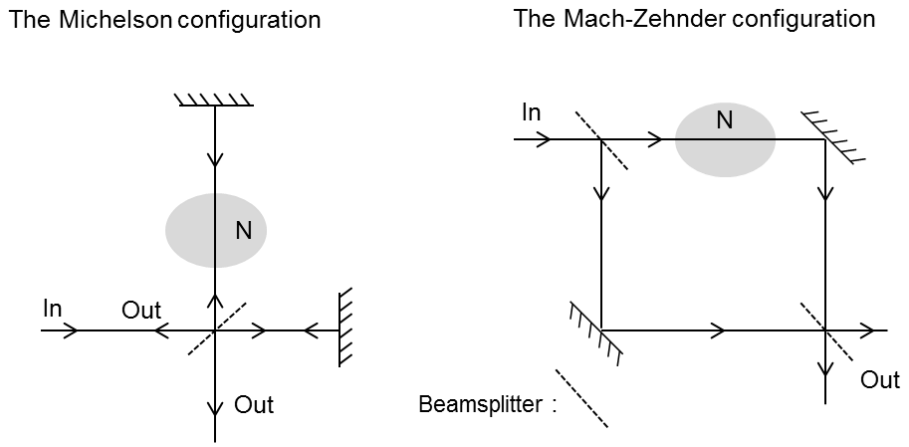

Figure 2.2 (left) the Michelson interferometer configuration (right) the Mach-Zehnder configuration [2].

2.3 Quasi-optics theory

In millimeter and submillimeter wavelengths, lights are limited in their angular resolution by the wave nature of light. At much higher wavelengths than those waves, beam spreading due to diffraction is so severe that propagation is restricted almost exclusively to guided mode systems. At shorter wavelengths, diffraction is relatively unimportant, and system design is generally carried out within the framework of geometrical optics [11].

For the waves in this range, millimeter and submillimeter, the solutions to the wave equation are a set of Gaussian beam modes for a system symmetric about the axis of propagation. If one assume that the radiation contains z-dependence in an expression of the form $\exp(-ikz)$, the lowest-order, or fundamental Gaussian mode has the electric field distribution as,

$$\psi(z) = A\frac{\omega_0}{\omega(z)} exp\left[\frac{-r^2}{\omega^2(z)}\right] exp(-ikz) exp\left[\frac{i\pi r^2}{\lambda R(z)}\right] exp\left(i\, arctan\frac{\lambda z}{\pi\omega_0^2}\right) \quad (2.20)$$

where $r = (x^2 + y^2)^{1/2}$. The quantity ω is the beam radius (or spot size) and a function of *z*, the distance from the beam radius, which is illustrated in Figure 2.3 (left).

$$\omega(z) = \omega_0\left[1 + \left(\lambda z / \pi\omega_0^2\right)^2\right]^{1/2} \quad (2.21)$$

R is radius of curvature, which is also a function of z,

$$R(z) = z\left[1 + \left(\pi\omega_0^2 / \lambda z\right)^2\right] \quad (2.22)$$

At the beam waist, the radius of curvature is infinite, so the wave fronts are plane. Far from the beam waist, the beam radius and the radius of curvature both grow linearly with z, as for a spherical wave in geometrical optics emanating from a point source [17-20].

For most quasi-optical system focusing the beam is necessary. Via the

focusing element, the radius of curvature changes, which enables to create new beam waist. As illustrated in Figure 4.1 (right), the two beam waists are located at distances d_1 and d_2 from the focusing element, and they have waist radii ω_{01} and ω_{02}, respectively. Gaussian beam transformation equations give the distances to the waists

$$d_2 = f\left[1+\frac{d_1/f-1}{(d_1/f-1)^2+(\pi\omega_{01}/\lambda f)^2}\right] \tag{2.23}$$

In addition, relation between two beam waists are given as below,

$$\omega_{02}/\omega_{01} = \left[\left(d_1/f-1\right)^2+\left(\pi{\omega_{01}}^2/\lambda f\right)^2\right]^{-2} \tag{2.24}$$

, where f is focal length of optical element, lens.

In the microwave electronics system of the interferometer, first beam waist is located inside of horn antenna. With the horn parameter ρ and the approximation $\omega(z)=0.35a$ for rectangular horn antenna which have aperture dimension a, beam waist in Figure 2.4 could be determined and also position z could be obtained according to following equations: [11]

$$\omega_0 = \frac{\omega}{\sqrt{1+\left(\frac{\pi\omega^2}{\lambda R}\right)^2}} \tag{2.25}$$

$$z = \frac{\pi\omega_0}{\lambda}\sqrt{\omega^2-\omega_0^2} \tag{2.26}$$

. This position z is important when determining distance between lens and first beam waist, since it gives more precise result than assuming beam waist position as horn aperture.

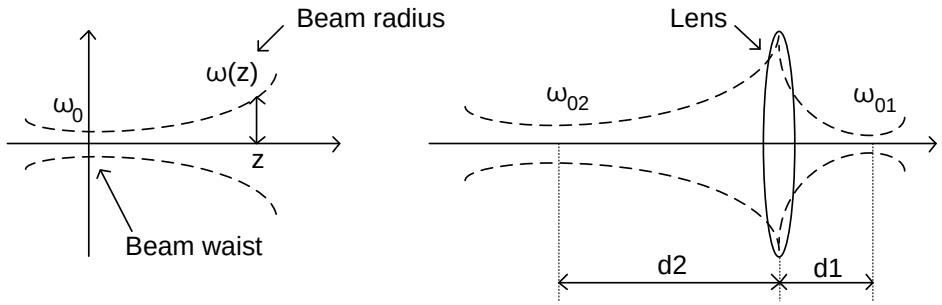

Figure 2.3 (left) Gaussian beam parameters: minimum beam radius corresponds to beam waist (right) Gaussian beam focusing parameters relation between beam waists and distance between beam waist and focusing parameter, lens.

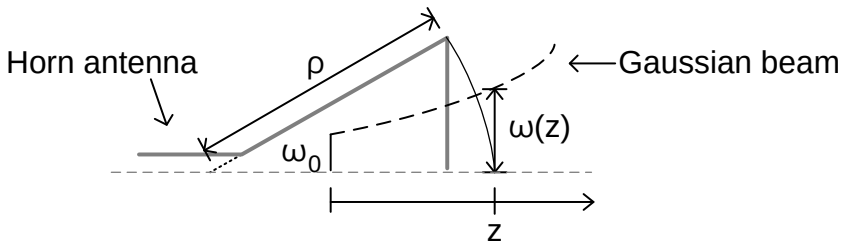

Figure 2.4 Determining process of beam waist from rectangular horn antenna parameter ρ. Beam radius at the point z is given by $0.35a$, where a is aperture of horn antenna and beam radius at z equals ρ.

Chapter 3 Overall system design

3.1 Design requirements

Prior to design the interferometer system for the VEST, design main parameters and requirements of the VEST system should be addressed. These will be used not only for overall system design process in the next section, but also for particular frequency or optical elements optimizing process in the following chapters.

Since interferometer measures plasma density basically, peak density value and density resolution should be given. For the first phase of operation, plasma current of the VEST is expected to 30 kA. Thus according to Greenwald limit [21], an operational density limit is given by

$$n_G = I_p / (\pi a^2) \sim 1 \times 10^{19} / m^3 \tag{3.1}$$

. Thus plasma peak density for the first phase of operation corresponds to $1 \times 10^{19}\ m^{-3}$. And density resolution is set as 10 % of its peak density according to the general value, thus required density resolution is calculated as 10 % of total line integrated density.

As an important requirement, spatial resolution of the system is set to 35 mm for small chamber of both upper and lower chamber, with considerations of radius of inner reflecting mirror. Since width of inner reflecting mirror is restricted by limiter, spatial resolution should be higher than the resolution that the mirror could include.

These parameters and requirements are summarized in Table 3.1. These function as limit conditions in wave frequency selection and beam focusing system design process.

Parameters	Value (for First phase)
Chamber dimension [m]	Main chamber: Φ 1.6 (D) x 1.2 (H) Small chamber: Φ 1.2 (D) x 0.6 (H)
Major radius [m]	0.4
Minor radius [m]	Main chamber: 0.3 Small chamber: 0.15
Plasma current [kA]	30
Peak density [m^{-3}]	1×10^{19}
Total line integrated density [m^{-2}]	Main chamber: 1.2×10^{19} Small chamber: 0.6×10^{19}
Required density resolution [m^{-2}]	Main chamber: 1.2×10^{18} Small chamber: 0.6×10^{18}
Average path length change due to vibration [mm]	~0.01
Fringe resolution	~1E-15
Spatial resolution	Small chamber : 35 mm
Temporal resolution	1.67E-8 [sec]

Table 3.1 Main parameters and requirements of the VEST device

3.2 Overall system design

As a diagnostic system, an interferometer compares phase shifted probing beam with reference beam, thus basically beam electronics system is needed in order to generate, launch, receive, and compare the beam. Although some systems set beam antenna inside the device, since this has both align and vacuum problem, usually *probing beam is launched from horn antenna into the plasma through passing the window*.

Receiver horn antenna is able to be located any position where probing beam could reach, and the path from launching antenna to receiving antenna becomes integration path. However for the VEST device, long path using two different windows as launching and receiving window diverges the beam a lot due to both wavelength range and system geometry, and also it requires long waveguide which reduce transmitted power. Therefore *double-path interferometer system* which utilizes inner mirror as reflecting material is designed for VEST, as shown in Figure 3.1.

Initial operation of the VEST will focus on double null merging start-up schemes using two partial solenoid coils installed at both vertical ends of a center stack. In order to understand plasma behaviors of the VEST, evolution of density profile is an important plasma parameter to be diagnosed. Therefore, the interferometer system to *measure line integrated plasma densities at several horizontal planes* needs to be employed.

Measurement of line integrated plasma densities at several horizontal planes could actually be done using multi chord measurement system which uses several interferometer modules. However, since the VEST plasma can be assumed as uniform at several shots with identical conditions, *the single chord measurement configuratio*n in Figure 3.1, of which both beams of double-path are lie in horizontal plane, *can measure several shots by moving vertically in repeating identical shots*. This measurement is also simple and economical to apply.

In single chord measurement of beams on horizontal plane, refraction effect will be significant because of its line of sight is about 1000 mm and usually it will use millimeter wave in this device at initial phase. However, due to its low aspect ratio with inner limiter, size of inner reflecting mirror is restricted to about 35 mm for the small chamber case. Therefore with low spatial resolution, it cannot only reflect the beam well, but also the results will not be reliable. Therefore, for the VEST geometry, *beam focusing system is necessary* to be developed.

Because the interferometer beam is launched outside the window, it is easy to install beam focusing system outside the window, between window and antenna. In this case, two types of focusing systems are available; one uses planar mirrors and concave mirrors and the other uses plano-convex lenses in front of the horn antenna. The former [15, 16] has the advantage of ease of development but occupies a large volume while the latter has the advantages of being compact and easy to align. Thus, *the configuration with the plano-convex lenses was chosen for VEST, where a large volume for the focusing system is not available.*

In conclusion, the *VEST interferometer system comprises microwave electronics system and beam focusing system*, as shown in Figure 2.1. Its single chord configuration can be used as vertically moving measurement, as shown in Figure 2.2. Also beam focusing system is necessary for vertically moving measurements though, its beam focusing system is not identical since vertical moving measurement should use cylindrical inner mirror, which cannot focus the beam on plane vertical to cylinder. Therefore, optimum beam focusing system is needed for the vertical moving measurements separately, which will be addressed in the chapter 5.

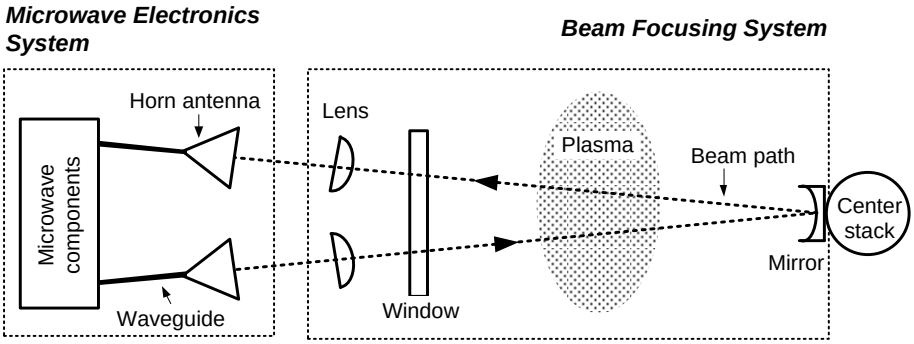

Figure 3.1 Top view of the overall interferometer system arranged on the VEST. The dotted line shows the probing beam path through the plasma.

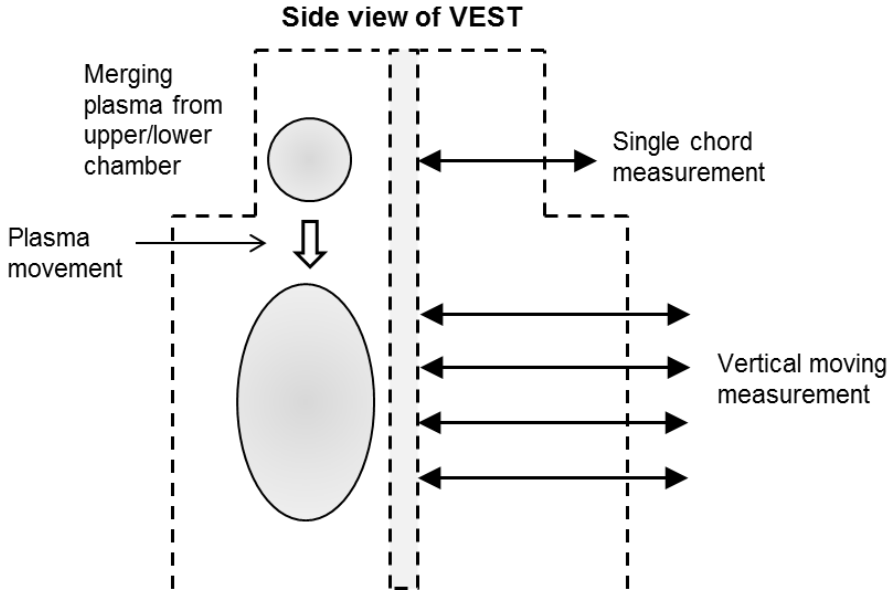

Figure 3.2 Side view of VEST: Single chord measurement configuration and vertical moving measurement which measures line integrated density in repeating identical shots.

Chapter 4 Microwave electronics system

In this chapter, developing process of microwave electronics system is explored. Based on the basic equations of interferometer in Chapter 2.3, selection of optimum frequency for the VEST interferometer is discussed by limiting possible frequency range. Then heterodyne microwave system is described.

4.1 Frequency selection

Interferometer launches electromagnetic wave into the plasma, by which phase of electromagnetic wave is shifted proportional to the plasma density. According to dispersion relations, since wave frequency and wavelength are determined by plasma property such as density, appropriate frequency of electromagnetic wave should be chosen in order to function well as an interferometer. Not only plasma property itself, but also the other factors affect on interferometer results, thus various constraints should be considered to select optimum wave frequency. Some frequency limitation factors are summarized in table 4.1, and these are discussed in the following sections.

Low frequency limits	High frequency limits
- Cutoff frequency - Refraction - Fringe jump	-Vibration -Resolution

Table 4.1 Frequency limits which determine optimum microwave for interferometer

4.1.1 Low frequency limits

Three factors play an important role as low frequency limits; cutoff frequency of the plasma, refraction effect due to plasma density gradient and fringe jump to due to significant change of density. Among these, cutoff frequency is fundamental factor since waves with frequencies lower than cutoff frequency could not transparent the plasma. Cutoff frequency is given as [8],

$$\omega_c = \sqrt{\frac{n_e e^2}{\varepsilon_0 m_e}} \tag{4.1}$$

, thus it is proportional to plasma density. Therefore, high frequency waves should be used for high density plasmas.

From Equation (4.1), the operational density limit given by Greenwald limit for the first phase of VEST operation is $10^{19} m^{-3}$. Therefore, corresponding cutoff frequency is 28 GHz, thus frequency of wave should be higher than this frequency.

In addition to cutoff frequency, deflection due to plasma density gradient also affects low frequency limits. The maximum deviation of the beam position due to refraction is given by [9]

$$R_0 \times \alpha_m = R_0 \times (8.97 \times 10^{-16}) \times n_0 (c^2 / f^2) \tag{4.2}$$

, where R_0 is the major radius, α_m is the angle difference between the incoming and outgoing beams through the plasma region, n_0 is the peak density, c is the speed of light and f is the frequency of the wave.

Figure 4.1 represents deflection at both upper and main chamber, and deflection in the main chamber is larger than the upper chamber since wave path length is longer in the main chamber. In the VEST geometry, inner reflecting mirror width is restricted due to limiter, yet if deflected beam could

be placed inside of circular mirror, then deflection is allowable. In the VEST upper chamber, deflection lower than 4 mm is allowable, thus wavelength lower than 4 mm is appropriate in Figure 4.1.

Also, fringe jump due to sudden change of density restricts wave frequency. If fringe of line integrated density changes more than half fringe, it is impossible to know whether this fringe change is due to density increase or decrease, without the aid of phase comparator. Therefore, density change corresponds to half fringe becomes allowable maximum density change. In Figure 4.2, waves of several millimeter wavelengths correspond to several $10^{20} m^{-3}$ density, which is higher value than maximum density in the VEST. Therefore, millimeter waves do not allow fringe jump to happen.

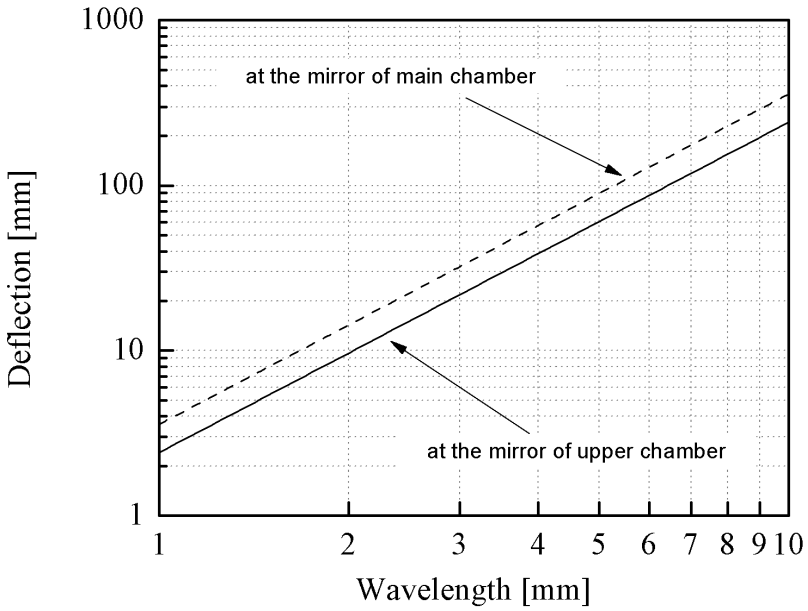

Figure 4.1 Deflection of beam due to plasma density gradient increases at high wavelength, i.e. low frequency, thus higher frequency is preferred to reduce deflection.

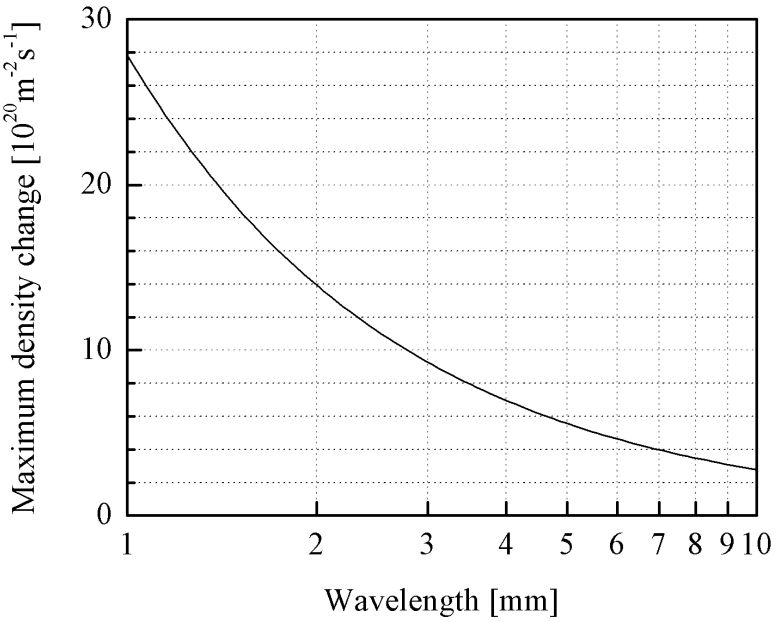

Figure 4.2 Allowable maximum density change which corresponds to half fringe, decreases at high wavelength, i.e. low frequency.

4.1.2 High frequency limits

There are two factors which restrict high frequency limit: path length change due to vibration and resolution of measured density. At first, if resolution of line integrated density is given, vibration limit could be determined as the path length change according to this resolution.

If path length of Δl is varied due to the vibration, corresponding fringe variation becomes $\Delta F = \Delta l / \lambda$, then changed path length by vibration could be given as

$$\Delta l = 4.49 \times 10^{-16} \lambda^2 \int n_e dl \tag{4.3}$$

If the resolution of line integrated density is set as 10 % of its maximum value, vibration limit becomes 10 % of above path length change with maximum density condition.

Using the maximum density given in the previous section from Greenwald density limit and assuming parabolic density profile for upper chamber geometry, vibration limits are presented in Figure 4.3. Results show that vibration limit decreases as wavelength decreases, i.e. frequency increases. Thus at high frequencies much attention should be paid on waves about vibration induced problems. In general, path length change is known as about several micrometers, waves in millimeter wavelength range are free enough from vibration problems.

As shown in Figure 4.3, resolution of measured density not only determines vibration limit, but also determines high frequency limit. Fringe number of phase shift is given by

$$F = \Delta\phi / 2\pi = 4.49 \times 10^{-16} \lambda \int n_e dl \tag{4.4}$$

. According to this equation, line-integrated density of one fringe

increases at higher frequency, and it is represented in Figure 4.4. Hence resolution of measured line-integrated density becomes worse at high frequency, thus this limits high frequency. Since the maximum plasma density at the VEST is expected to be about $10^{19} m^{-3}$ from Figure 4.4, waves in millimeter wave range are free of resolution problem with regard to the resolution of this system.

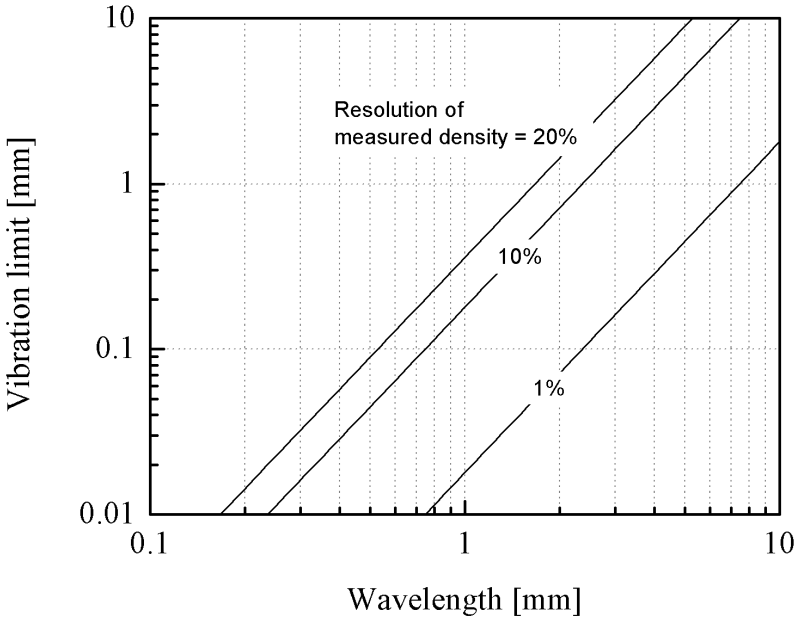

Figure 4.3 Vibration limit decreases with high frequency, thus at high frequencies much attention should be paid to waves about vibration problem.

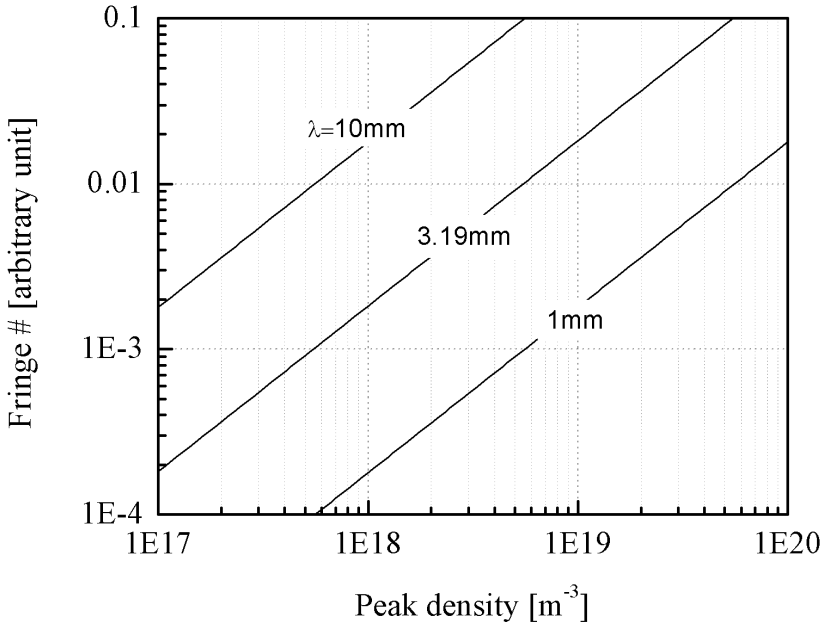

Figure 4.4 At lower wavelength, i.e. higher frequency, line integrated density which corresponds to one fringe increases, thus resolution of measured density becomes worse.

4.2 94 GHz microwave electronics

From the previous section, for the initial phase of the VEST, waves in millimeter range about from 1 mm to 4 mm, satisfied all limitation conditions. This range corresponds to waves of frequency from 75 GHz to 300 GHz. And cutoff density for these waves ranges about from $7\times10^{19}m^{-3}$ to $112\times10^{19}m^{-3}$, all above the maximum density limit of the VEST. Therefore, in this frequency range, available 94 GHz electronics system is chosen as a microwave heterodyne system, which had been developed for RAPID device [22].

The schematic diagram of the microwave electronics for the 94 GHz heterodyne interferometer system is shown in Figure 4.5. Two Gunn oscillators with a 94 GHz operating frequency are used in a heterodyne configuration; one is voltage-controlled and the other is mechanically controlled. Isolators are used for both oscillators to prevent power from propagating back to the oscillators. The two mixers generate the reference signal and probe signal with an intermediate frequency of 60 MHz, and these signals are transmitted by a coaxial cable to detectors such as an oscilloscope or phase detector. The overall system is shielded by an aluminum box and will be located more than 50 cm away from the device to reduce the effect from the magnetic field on the microwave components.

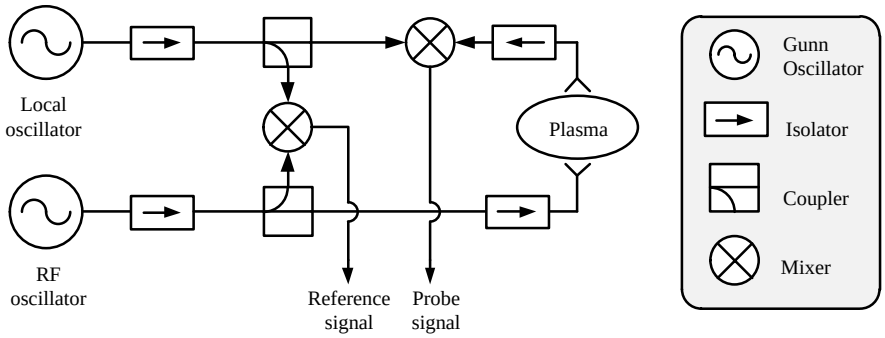

Figure 4.5 Schematic diagram of the 94 GHz heterodyne interferometer system

Chapter 5 Beam focusing system

From the previous chapter, 94 GHz microwave is chosen as the VEST interferometer wave frequency for the first operation phase. 94 GHz wave has a wavelength of 3.2 mm, which lies in millimeter wave range, thus quasi optical approach should be applied to this wave of high diffraction. In this chapter, beam focusing system is designed for the VEST interferometer based on quasi-optics theory (Chapter 2.3) in order to increase spatial resolution thus generate phase shift more effectively. According to measurement configurations addressed in chapter 3, beam focusing system is designed for both single chord measurement configuration and vertical moving measurement configuration. In the first phase of operation, single chord measurement configuration will be used in advance, so beam focusing system for single chord measurement configuration has been fabricated and tested to verify its ability of beam focusing.

5.1 Optical elements design

5.1.1 System requirements

Since millimeter wave in the VEST interferometer has relatively large refraction effect as discussed in the previous chapter, appropriate beam focusing system is necessary in order to enhance efficiency of the system. Two main objectives of beam focusing system are: converging Gaussian beam in order to reduce power low due to diverging beam and locate beam waist at plasma center in order to determine phase shift more effectively. To achieve these goals, ray tracing simulations should be done to design optimum optical elements- lenses and mirror- for specific configurations. Every beam focusing system comprises focusing lenses and inner reflecting mirror.

In the chapter 3, measurements are discussed for single chord measurement and vertical scanning measurement. Although both measurement configurations are based on single chord horizontal plane configuration, system requirements are different since their aims are difference.

At first, in single chord measurement, two measurement plans are possible with same configuration since rotating horizontal configuration 90 degrees directly corresponds to vertical configuration. However, horn antenna must not rotate in order to keep E-plane of the beam parallel to toroidal magnetic field direction. In this measurement configuration, with a assumption of circular transverse beam shape, inner reflecting mirror should be circular shape in order to place beam waist of both E-plane and H-plane at the plasma center. In addition, the other advantage of circular mirror is that it could be applied to both horizontal and vertical configurations. In other words, identical beam focusing system could be utilized for both horizontal and vertical configurations of single chord measurements.

In vertical scanning measurement plan, horizontal plane configuration of single chord measurement would be applied, yet identical beam focusing system is not available. This is because circular mirror could not be applied for vertical scanning measurements. Instead, cylindrical mirror could act as a reflecting mirror. However, cylindrical mirror can focus the beam on E-plane, thus Gaussian beam on H-plane is reflected at mirror and diverges. In this case, Gaussian beams on E-plane and H-plane should be analyzed separately and also beam focusing system should be designed differently as similar previous study did using cylindrical lenses [23]. For Gaussian beam on E-plane, identical approach utilizing cylindrical lenses would be applied as single chord measurement, but Gaussian beam on H-plane requires different approach. Because diverged beam from plasma center could not be focused after reflection, reducing loss of the diverging plays an important role. Therefore, instead of locating beam waist at plasma center, locate beam waist at mirror position for Gaussian beam on H-plane. Although this sacrifices

effective phase shift by locating beam waist at plasma center a bit, eventually it enhances phase shift efficiency by converging reflected beam.

With regard to these requirements above, summarized requirements for beam focusing system of different configurations are given in table 5.1.

	Lens	**Mirror**
Single chord measurement	- function as focusing element -circularly shaped - place beam waist at plasma center	- circular mirror -focusing beam to plasma center
Vertical scanning measurement	- function as focusing element - cylindrically shaped - different for E/H-plane - E-plane: place beam waist at plasma center - H-plane: place beam waist at mirror	- cylindrical mirror -E-plane:focusing beam to plasma center - H-plane: no focusing, only reflecting

Table 5.1 Role of lens and mirror in beam focusing system of different measurement configurations

5.1.2 Single chord measurement system

A compact beam focusing system for single chord measurement utilizing a pair of plano-convex lenses and a concave mirror is designed to maximize the effective beam reception and spatial resolution. A beam path analysis based on quasi-optics is used in the design of the beam focusing system to locate the beam waist at the plasma center, which more effectively allows generating a phase shift in the plasmas.

In order to focus a beam, plano-convex lens of which consists of plane and convex sides is chosen. Polytetrafluoroethylene (PTFE) generally known as Teflon is chosen for the lens material, since it is easy to fabricate and has reasonably low dielectric absorption. The fractional power transmitted through a thickness l of low-loss material having dielectric function $\varepsilon = \varepsilon' - i\varepsilon''$ ($n = \sqrt{\varepsilon'}$) and loss tangent δ ($\tan\delta = \varepsilon''/\varepsilon'$) is given by [11]

$$f_T = \exp[-(2\pi/\lambda_0)nl\tan\delta] \tag{5.1}$$

Since dielectric constant for Teflon is 2.06 and loss tangent is 2×10^{-4} at the frequency of 90GHz, $f_T \sim 0.996$, it is reasonable to use it.

The schematic of the designed beam focusing system with the two Teflon plano-convex lenses in front of the horn antennas and a concave reflecting mirror inside the vacuum vessel is shown in Figure 5.1. Due to the geometrical limitations of the device, two plano-convex lenses will be installed outside the chamber, between the horn antenna and the window.

To design the optical components, a quasi-optics approach was taken rather than using geometrical optics since the microwave beam has its wavelength in the millimeter range, as mentioned in the previous section. The two plano-convex lenses focus the diverging beam to form a beam waist at the plasma center. The concave mirror reflects the beam to the receiving horn antenna and also focuses the beam to form a beam waist at the plasma center; thus, the sending beam and reflected beam exhibit a symmetrical profile as

shown in Figure 5.1.

The design parameters of the Teflon lenses are characterized by their focal lengths and diameters. For a plano-convex lens with a curvature radius *R*, the focal length is given by

$$f = \frac{R}{n-1} = \frac{R}{0.44} \tag{5.2}$$

, where the refractive index (*n*) of the Teflon is given by 1.44 at 90 GHz [17]. As shown in Figure 5.1, the distance between the lens and the first beam waist, d2, must exceed 200 mm in order to locate the first beam waist at the plasma center. According to Gaussian optics, d2 can be expressed by the distance between the horn antenna and the lens, d1, following [17]:

$$\begin{aligned} \mathrm{d2} &= f + (\omega_{02}/\omega_{01})(f^2 - f_0^2)^{1/2} \\ &= R/0.44 + (\omega_{02}/\omega_{01})((R/0.44)^2 - (\pi\omega_{01}\omega_{02}/\lambda)^2)^{1/2} \\ &= f\left[1 + \frac{\mathrm{d1}/f - 1}{(\mathrm{d1}/f - 1)^2 + (\pi\omega_{01}{}^2/\lambda f)^2}\right] \end{aligned} \tag{5.3}$$

, where ω_{01} is the first beam waist radius; λ is a 3 mm wavelength, and $f_0 = \pi\omega_{01}\omega_{02}/\lambda$. The beam waist radius at the sending horn antenna, ω_{01} , can be calculated from the physical size of the horn antenna as 4.8 mm [11]. The calculated results of the lens design parameters are shown in Figure 5.2, where the relationship between (a) d2 and the first beam waist radius, (b) d2 and d1, (c) the beam radius at the mirror and the first beam waist radius, and (d) the beam radius at the lens and d1 are plotted. The optimum curvature radius of the lens, *R*, can be determined from these relationships with some geometrical constraints.

The first constraint is that d2 must exceed 200 mm; thus, the available beam waist radius and curvature radius of the lens were determined from Figure 5.2 (a). This constraint also gives the available range of d1 and the curvature radius of the lens in Figure 5.2 (b). In addition, since the beam radius at the mirror should be shorter than 40 mm due to the VEST geometry,

this also limits the available beam waist range at the plasma center in Figure 5.2 (c). Lastly, since the two lenses will be installed in front of one vacuum window one by one and the radii of these lenses should be larger than the beam radius at the lenses, the beam radius at the lenses should be less than 30 mm, which is a quarter of the width of the vacuum window. This beam radius yields the proper range of d1 from Figure 5.2 (d). From all these constraints, lenses with a curvature radius of 43 mm were found to be suitable for the VEST interferometer system.

The inner reflecting mirror was designed to locate the reflected beam waist to the plasma center shown in Figure 5.4. Thus, a spherical concave mirror with a curvature radius of 540 mm was selected to locate the focal point at the plasma center (270 mm from the mirror). If the first beam waist is located at the plasma center, the focal point of the mirror, the reflected beam waist will also be located at the plasma center. Since the inner reflecting mirror was installed on the inner wall of the VEST chamber, it can be exposed to the plasma. Therefore, it should be either installed behind the limiter or play a role in the limiter itself. This as well as the beam radius at the mirror was used to determine the mirror diameter.

Stainless steel 316L, the VEST chamber material, is used as mirror material since its fractional power loss per reflection from a metal surface is reasonably low by the formula below;

$$f_L = 2.1\times10^{-4}[\, f(GHz)/\sigma(10^7 S/m)]^{1/2} \qquad (5.4)$$

where σ is the conductivity and f is the frequency. Thus in our case, $f_L \sim 0.001$, which enables to use it as a reflecting material.

In addition, the optimum distances d1 and d2 can be determined from Figure 5.2 (b). To install the interferometer system on VEST, the distance from the lens to the window should be longer than 30 mm, i.e. d2 should be longer than 230 mm, because of the flanges on the device. Furthermore, since a shorter d1 is preferred from Figure 5.2 (d), a d1 of 108 mm and d2 of 242

mm were determined as the optimum distances; thus, the total distance from the antenna to the mirror is 620 mm (d1+d2+270=620 mm). With these values and the designed beam focusing system, the beam radius and beam intensity ratio along the beam path were calculated shown in Figure 5.3. After the beam transmits through the lens, the first beam waist is formed at the plasma center and the beam radius at the mirror becomes less than 25 mm, which is 6 times less than that without the focusing system. Therefore the spatial resolution with beam focusing system is 6 times better than that without beam focusing system. The diameter of the reflecting mirror was determined as 70 mm with a sufficient margin.

As expected, the beam intensity ratio increases after it transmits through the lens and its intensity ratio at the mirror is about 30 times larger than that without the focusing system. Therefore, with the beam focusing system, both the spatial resolution and beam intensity are expected to be significantly enhanced.

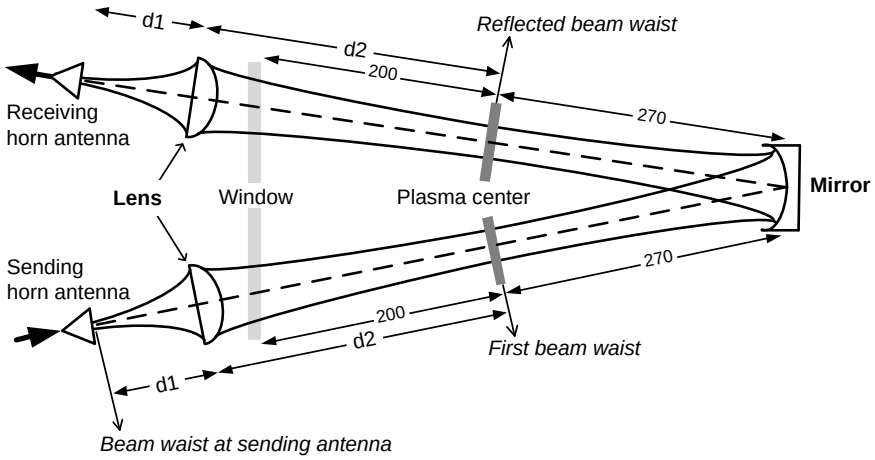

Figure 5.1 The horizontal view of the beam trajectory (broken line) with the beam radius (unbroken line) is shown for the designed beam focusing system from the sending horn antenna through the inner reflecting mirror to the receiving horn antenna (units in mm).

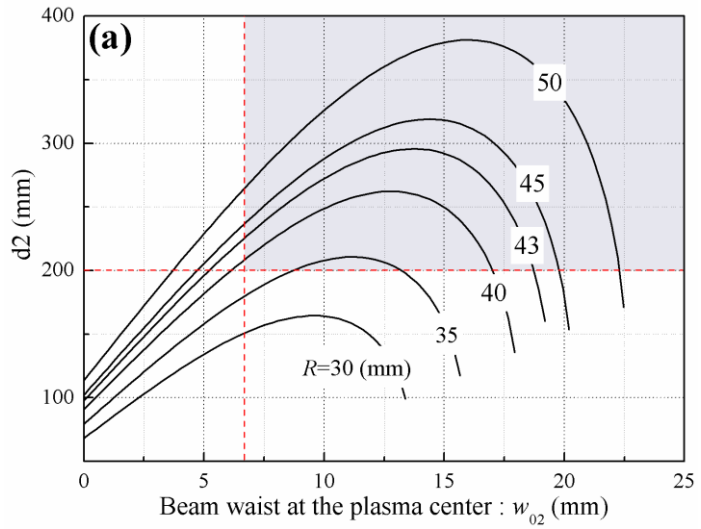
(a)
400
300
200
100
d2 (mm)
0
5
10
15
20
25
Beam waist at the plasma center : w_{02} (mm)
50
45
43
40
35
R=30 (mm)

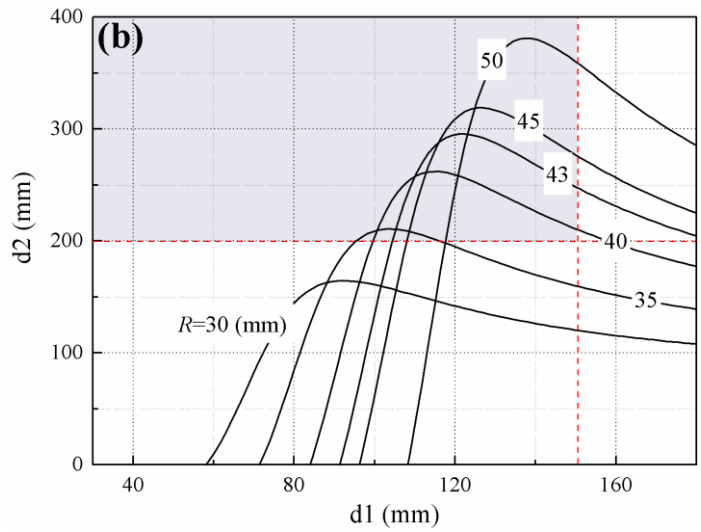
(b)
400
300
200
100
0
d2 (mm)
40
80
120
160
d1 (mm)
50
45
43
40
35
R=30 (mm)

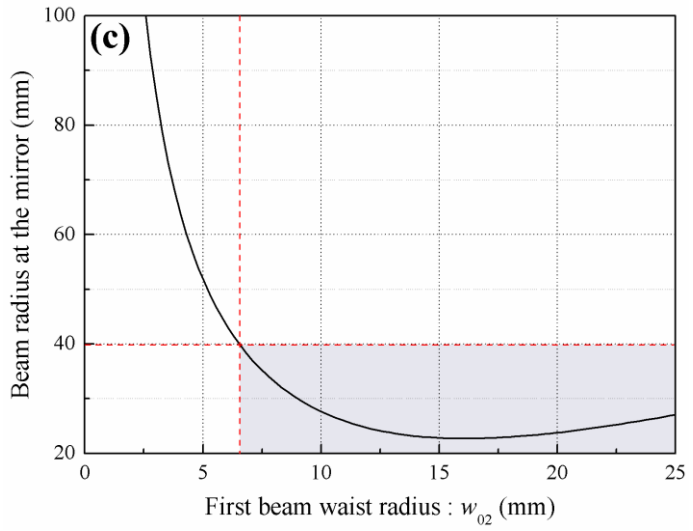

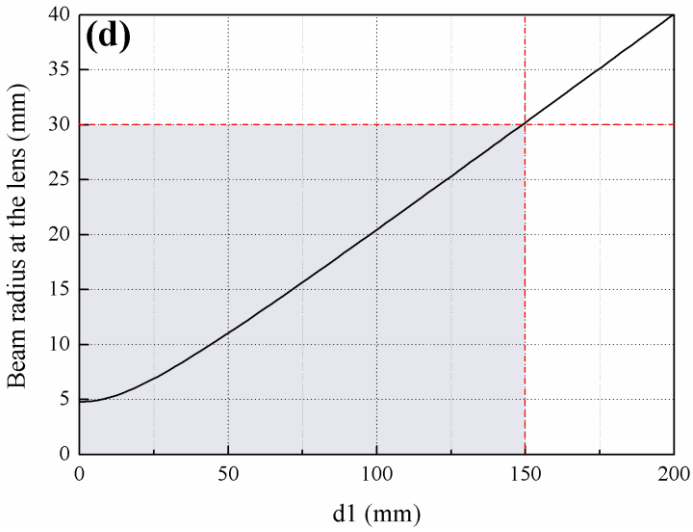

Figure 5.2 Calculated results of the lens design parameters show the relationship between (a) d2 and the first beam waist radius, (b) d2 and d1, (c) the beam radius at the mirror and the first beam waist radius and (d) the beam radius at the lens and d1 (*R*: lens curvature radius).

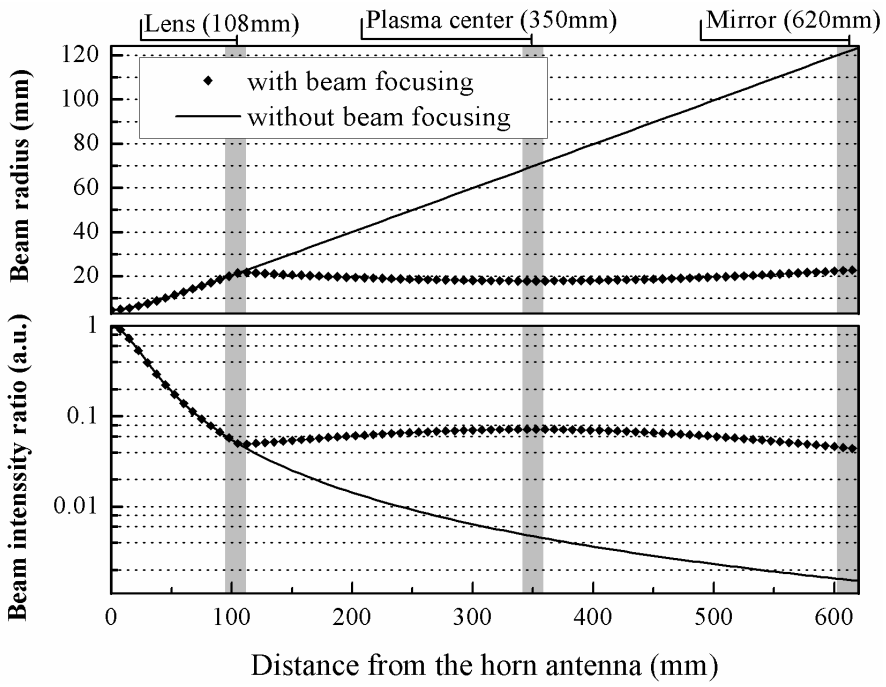

Figure 5.3 Calculated beam radius and beam intensity ratio along the beam propagation with the beam focusing system shows the spatial resolution with beam focusing system is 6 times better than that without beam focusing system

5.1.3 Vertical moving measurement system

In order to design a beam focusing system for vertical moving measurement configuration, both horizontal plane and vertical plane view are considered as required in chapter 5.1.1. To enable vertical scanning, cylindrical inner reflecting mirror is selected, thus top view and side view of the mirror are different as illustrated in Figure 5.4. For E-plane, horizontal plane, design constraints are identical as those of previous single chord measurement configuration, yet vertical plane configuration differs from it. Since mirror in vertical plane configuration does not work as focusing element, beam waist is designed to position at the mirror. Therefore two different cylindrical lenses are used to focus at different position, since 90 degree rotated cylindrical lens does not function as focusing element. This type of focusing system [23] could be utilized since the 2D Gaussian beams of E-plane and H-plane can be treated as independent of one another [11].

As did in the previous section, design of optical elements has been done to satisfy several constraints of the VEST system. With the aid of quasi-optics, positioning beam waist at plasma center on E-plane and at mirror on H-plane can be represented as

$$e2 + 3\,8\,0\,\theta\, f\left[+1\frac{e1/f - 1}{(e1/f -)^2 + \left(\pi\omega_{e1}{}^2 \quad \lambda f\right)^2}\right] \tag{5.5}$$

$$7\,8\,0\,\theta\, h \quad 2 \geq f\left[+1\frac{h1/f - 1}{(h1/f -)^2 + \left(\pi\omega_{h1}{}^2 \quad \lambda f\right)^2}\right] \tag{5.6}$$

where ω is beam waist, f is focal length of lens and λ is wavelength of beam. Therefore, in Figure 5.5, distance between horn antenna and window (e1+e2 for E-plane and h1+h2 for H-plane) is determined for different radius (R) of lenses depending on distance between horn antenna and lenses (e1 for E-plane and h1 for H-plane). Since the distance between horn antenna and window is identical for both planes in the experimental configuration, e1 and

h1, of which e1+e2 and h1+h2 satisfy identical value, become appropriate condition. A line of slope 1 corresponds e2=h2=0 condition, which lenses are located at window position, thus solutions must satisfy higher than this line.

To be specific, in order to find optimum lenses of a particular radius R, point A (R=85, e1=270 mm) and B (R=115, h1=318 mm) in Figure 5.5 have been selected since their vertical value is identical as 359 (mm) and high above line of slope 1. In addition, other constraints have also been considered to select these as optimum values, which are presented in Figure 5.6 and Figure 5.7.

Figure 5.6 shows diverging beam radius from horn antenna (beam waist) along propagation path for waves in E-plane (e1) and H-plane (h1). Since beam radius is limited due to limited geometrical condition, beam radius should be less than 40 mm. To satisfy this, both distance between horn antenna and lens (e1 and h1) should be less than 320mm. Also, for E-plane case, beam radius at the mirror should be less than a particular value considering limiter thickness, and mirror is designed based on beam radius at the mirror position. This could be determined from Figure 5.7, in which calculated beam radius at mirror position depending on distance between horn antenna and lens for wave of E-plane show different result for different lens radius *R*.

From the result of Figure 4.7 which determined optimum distance for both lenses which lie in E-plane and H-plane, beam radii are calculated for both systems with or without beam focusing system in Figure 4.12. Even before reflecting from mirror, the beam radius of unfocused beam is more than 5~7 times larger than that of focused beam. Dashed line corresponds to the beam on E-plane and dotted line corresponds to the beam on H-plane. As designed, the beam on H-plane is set to focus its beam waist at the mirror, instead of plasma center. However, the spatial resolution at the plasma center is higher than 30 mm, and the spatial resolution in overall system is about 40 mm, therefore this beam focusing system enable the system to move vertically (more than 300 mm) with allowable spatial resolution.

Similar to the calculation which had done in Figure 4.12, peak intensity is determined along beam path for interferometer system with or without beam focusing system in Figure 4.13. As expected, peak intensity with beam focusing system is significantly better, about 100 times than that of unfocused beam.

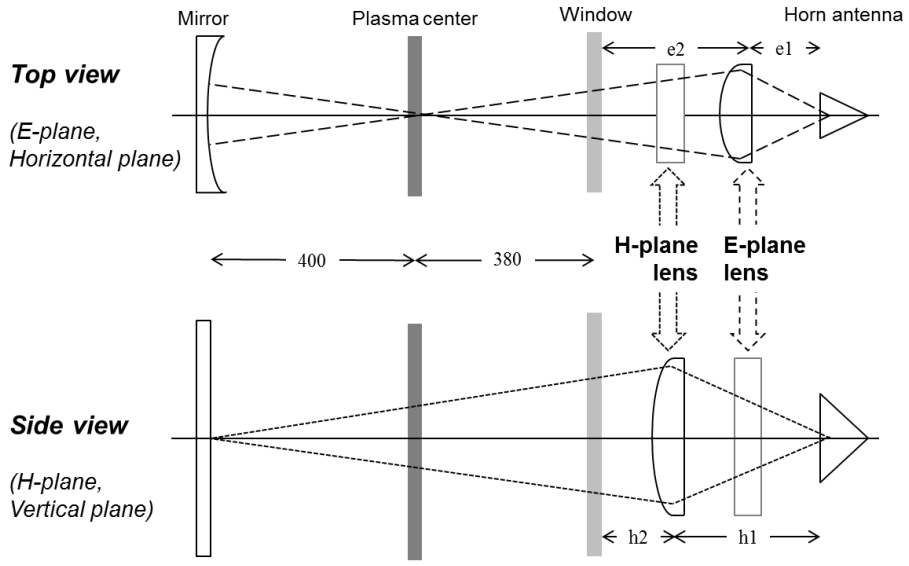

Figure 5.4 Design scheme of vertical scanning measurement system configurations for E-plane and H-plane. Top view shows E-plane configuration which is designed to place beam waist at plasma center. Side view shows H-plane which is designed to place beam waist at mirror. Important remark is cylindrical mirror functions as both focusing and reflecting mirror at horizontal plane, while it works as just reflecting mirror at vertical plane

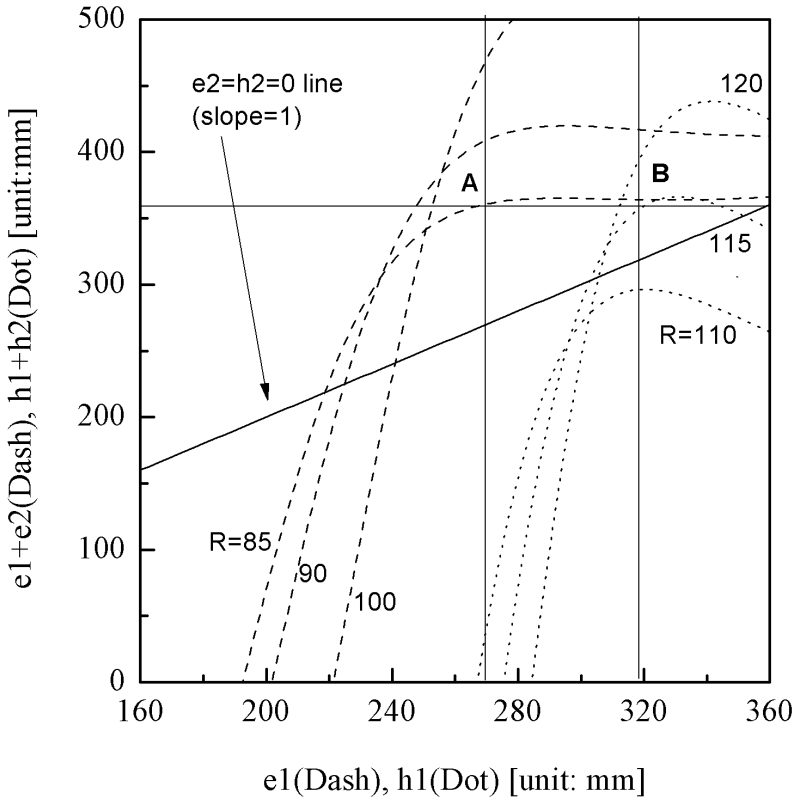

Figure 5.5 With the condition which locates beam waist at plasma center for E-plane and at mirror for H-plane, distance between horn antenna and window (e1+e2 for E-plane and h1+h2 for H-plane) is determined for different radius of lenses depending on distance between horn antenna and lenses (e1 for E-plane and h1 for H-plane). Since the distance between horn antenna and window is identical for both planes in the experimental configuration, e1 and h1 of which e1+e2 and h1+h2 satisfy identical value become appropriate condition. A line of slope 1 corresponds e2=h2=0 condition, which lenses are located at window position, thus solutions must satisfy higher than this line. Point A (R=85, e1=270 mm) and B (R=115, h1=318 mm) is selected as appropriate lens condition with other constraints.

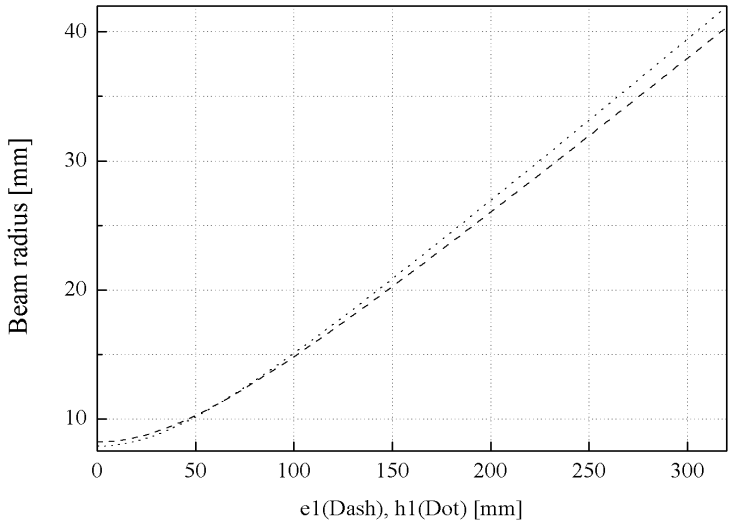

Figure 5.6 Diverging beam radius from horn antenna (beam waist) along propagation path for waves in E-plane (dash) and H-plane (dot).

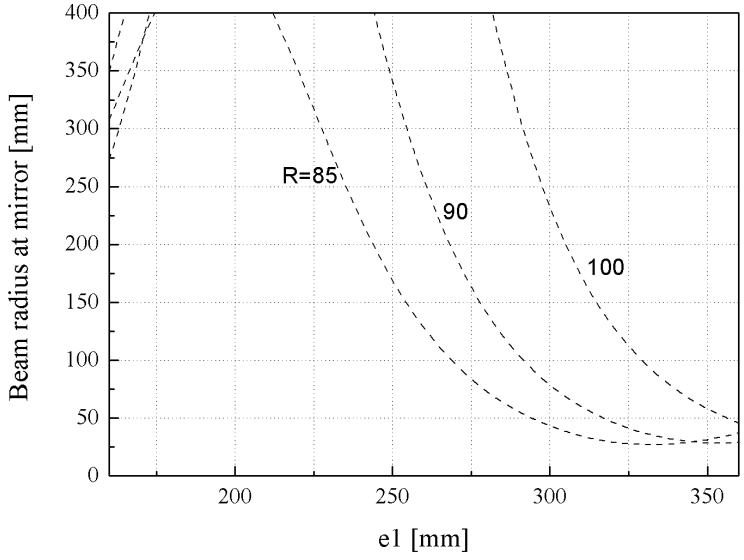

Figure 5.7 Calculated beam radius at mirror depending on distance between horn antenna and lens for wave of E-plane show different result for different lens radius *R*.

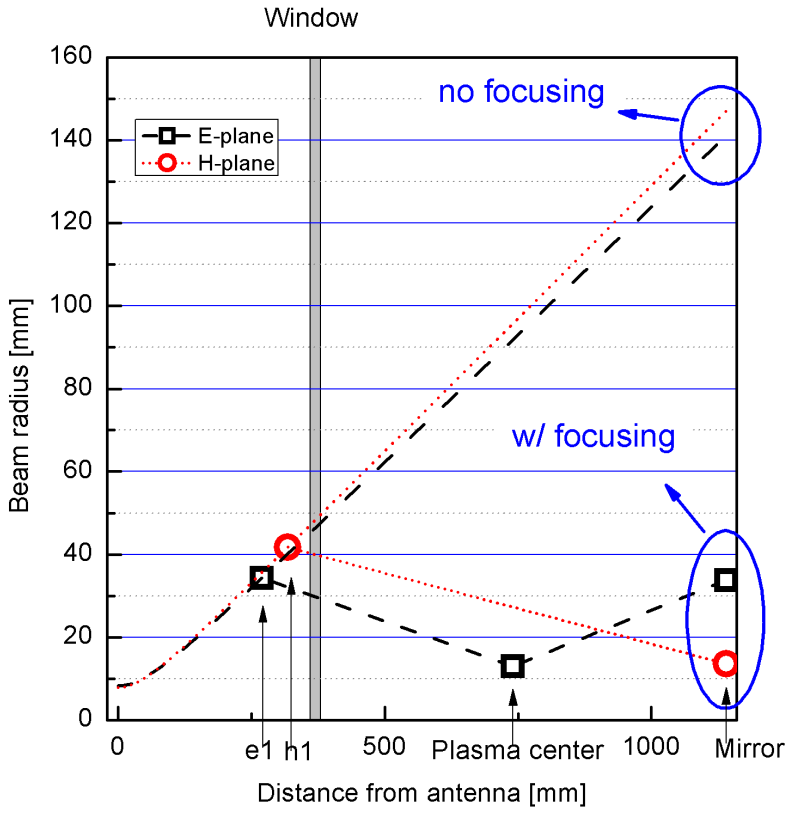

Figure 5.8 From the result of Figure 4.7 which determined optimum distance for both lenses which lie in E-plane and H-plane, beam radii are calculated for both systems with or without beam focusing system. Even before reflecting from mirror, the beam radius of unfocused beam is more than 5~7 times larger than that of focused beam. Dashed line corresponds to the beam on E-plane and dotted line corresponds to the beam on H-plane. As designed, the beam on H-plane is set to focus its beam waist at the mirror, instead of plasma center. However, the spatial resolution at the plasma center is higher than 30 mm, and the spatial resolution in overall system is about 40 mm, therefore this beam focusing system enable the system to move vertically (more than 300 mm) with allowable spatial resolution.

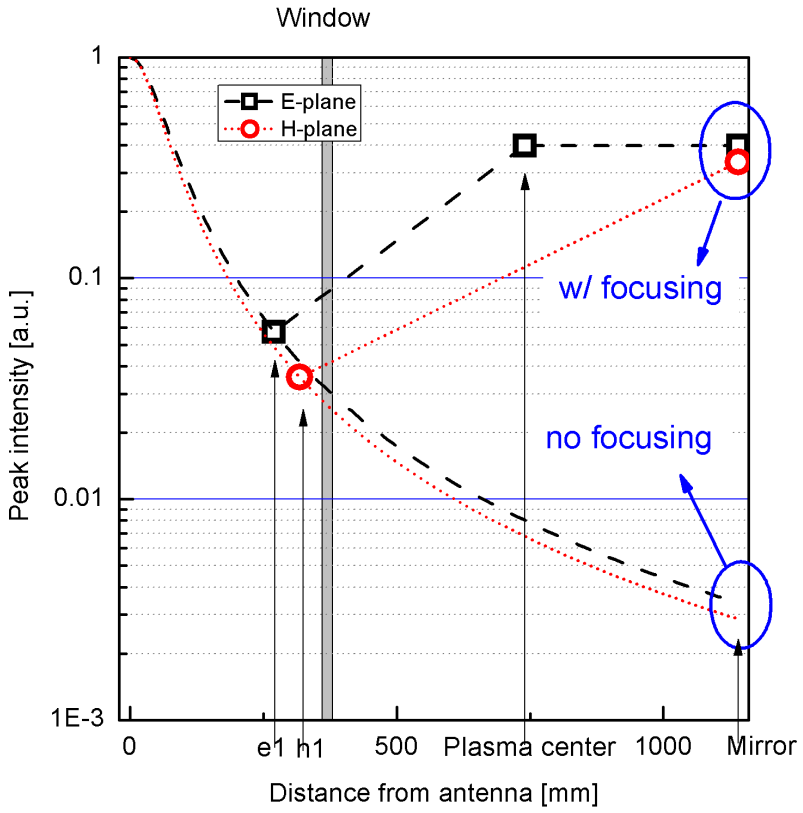

Figure 5.9 Similar to the calculation which had done in Figure 4.12, peak intensity is determined along beam path for interferometer system with or without beam focusing system. As expected, peak intensity with beam focusing system is significantly better, about 100 times than that of unfocused beam.

5.2 Beam focusing experiments

5.2.1 Experimental setup

Before installing the interferometer system on the device, preliminary experiments were done with the beam focusing system on a horizontal plane model reflecting a real-sized vacuum vessel, which is shown schematically in Figure 5.10. The distance from the antenna to the mirror was fixed at 620 mm and the calculated optimal values of d1, the distance from the antenna to the lens, and d2, the distance from the lens to the first beam waist, were 108 mm and 242 mm, respectively. Therefore, the distance from the mirror to the first beam waist was 270 mm, where the plasma center will be placed, using the optimal d1 and d2 distances (620-108-242=270 mm) at which the plasma center is located. If d1 is varied by moving the lens, d2 and ω_{02} will also vary according to the relationship shown in Figure 4.4. Thus, d1+d2, the distance from the antenna to the first beam waist, will deviate from the plasma center and this will result in poor beam focusing.

Two types of experiments were done. At first, by moving the lenses along the beam path, the optimum lens location (d1), which places the first beam waist at the plasma center, was determined from the position where the total beam intensity became the maximum value. The total beam intensity can represent the total beam power at the receiving antenna, not the beam intensity of the beam at the position where the beam profile is measured.

In order to verify the designed beam focusing system, the beam radii at several positions along the beam path were compared to the calculated ones in Figure 5.10; the beam profiles transverse to the beam path were measured. The knife-edge method [24], one of the Gaussian beam profile measurement methods generally used, was adopted. However, instead of a razor blade, which can reflect the beam into the receiving antenna, a 20 mm thick blocking plate made of a low reflectance Bakelite material was used, which is thick enough to absorb the beam. The blocking plate, which hardly transmits microwaves, was moved vertically downward at fixed increments of 5 mm to

partially block the beam. Thus, the total beam intensity at the receiver measures the integral of the remaining beam fraction, and the value decreases as the blocked area increases by moving the blocking plate downward. The vertical beam intensity profile can be obtained by differentiating the total beam intensities, and the beam radius is determined when the beam intensity decreases to $1/e^2$ of the peak intensity.

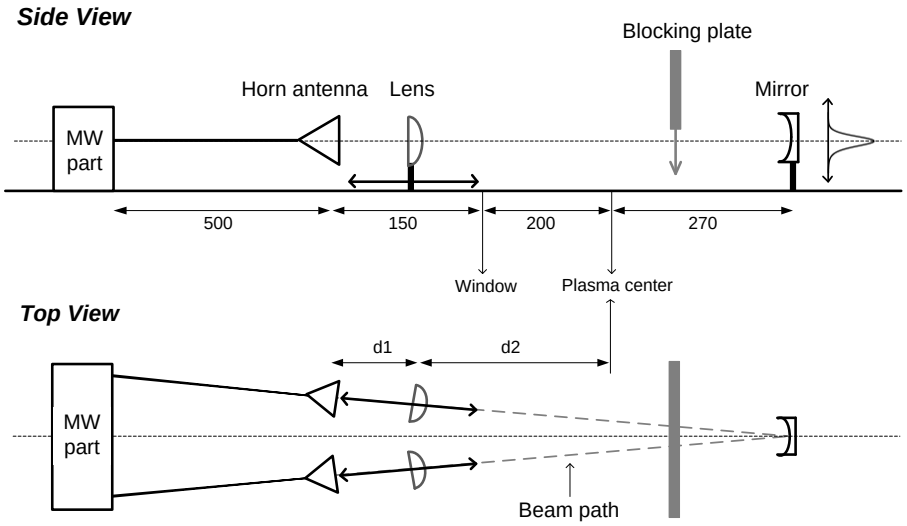

Figure 5.10 Schematic view of the experimental setup

5.2.2 Experimental results and discussion

When moving the lenses from the antennas to the window, the maximum total beam intensity was obtained at around 91 mm shown in Figure 5.11, and it was not much different from the calculated optimum value. This confirms that the Teflon lenses are working well as focusing elements. The reason for this variation is considered as the difference between the positions of the first beam waist and the reflected beam waist. It differs from Figure 5.11 in which both beam waists were placed at the plasma center. According to Figure 5.12, d2 varied with d1 when moving the lenses along the beam path; moreover, d1+d2 also varied in the calculated values shown in Figure 5.12 (up). It precludes the first beam waist to be located at the plasma center. Since the reflecting mirror is designed to have a focal length of 270 mm, which is the distance between the reflecting mirror and the plasma center, locating the reflected beam waist at the same position of the first beam waist is available only when the first beam waist is located at the plasma center shown in Figure 5.12. The distances of the first beam waist and the reflected beam waist from the mirror are plotted in Figure 5.12 (down). The result shows that the two distances have the same value of 270 mm when d1 is 108 mm. The positions of the two beam waists are different when d1 is not 108 mm; thus, it would be the reason for the variation in the total beam intensity. Even when the positions have a similar value to each other, the total beam intensity can vary since the lenses are designed only to focus the reflected beam when the beam waist is located at the plasma center.

From the results of this experiment, d1 was set at a position where the receiving total beam intensity had maximum value. Additionally, the beam profile measurements were done by moving the blocking plate downward in small increments into the beam in order to compare with the calculated beam radii along the beam path shown in Figure 5.3. As the blocking plate was moved downward, the total beam intensity decreased shown in Figure 5.13 (a) since the blocked beam cannot be received at the receiving antenna. Thus, the beam intensity profile transverse to the beam path can be obtained by

differentiating the polynomial-fitted total beam intensity shown in Figure 5.13 (a). The beam radius can be determined, where the beam intensity profiles shown in Figure 5.13 (b) decrease to $1/e^2$ of their peak intensities.

In order to compare the beam radii, measurements were done at three positions: at the vacuum window (after passing the focusing lens), at the plasma center (the focusing place where the beam waist was placed), and at the reflecting mirror, with the results shown in Figure 5.13. Since it is the normalized beam intensity profile, the narrower beam profile with a smaller beam radius showed higher peak intensity. The beam intensity profile at the plasma center showed the narrowest width and the highest peak intensity, which reflects that the beam is focused to have the lowest beam radius. In addition, the beam intensity profile at the mirror had the broadest width and the lowest peak intensity, which indicates that the beam diverges from the beam waist after passing the plasma center.

More beam profile measurements were done at various positions of the beam path, and the beam radii, where the beam intensity decreases to $1/e^2$ of its peak intensity, are plotted in Figure 5.14 on top of the calculated beam radii of Figure 5.3 for comparison. The results show that the beam radius deviated more from the calculated value as the distance from the mirror increased. The beam profile changing after passing through the blocking plate may be a possible reason for this discrepancy since the Gaussian beam profile is partially destroyed by the blocking plate. In this experimental configuration, the beam must propagate to the receiving antenna by transmitting other optical components after passing the blocking plate. Thus, the shorter propagation path after passing through the blocking plate may reduce the deviations. Since the beam is reflected at the mirror, placing the blocking plate near the mirror provides a shorter propagation path after passing through the blocking plate. Therefore, the deviation is smaller near the mirror.

Although there are some deviations between the experimental results and the numerical calculations, Figure 5.14 shows reasonable agreement in the

overall behaviors. The results show that the beam is focused by the lenses and then, diverges after the plasma center. In other words, the beam waist is located near the plasma center as designed; therefore, the beam focusing system performs well as expected.

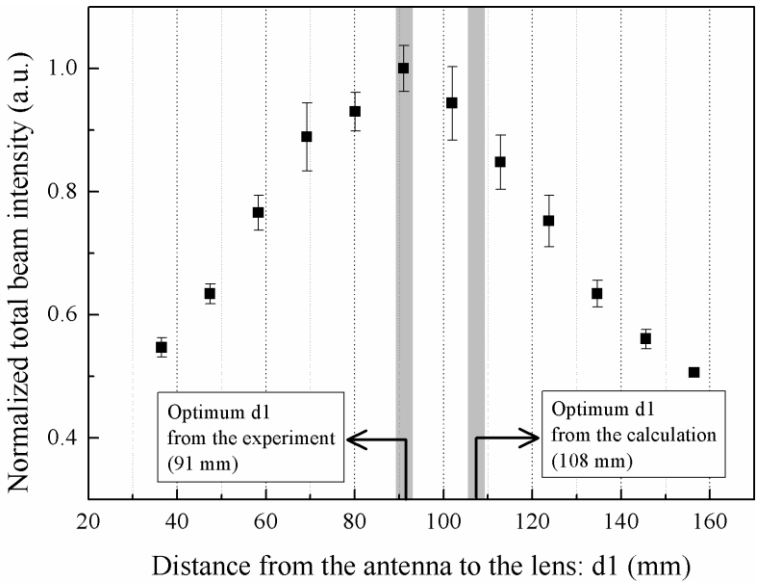

Figure 5.11 Normalized total beam intensity shows its maximum value near 90 mm while the calculated value for a constant d1+d2=350 mm system was 108 mm.

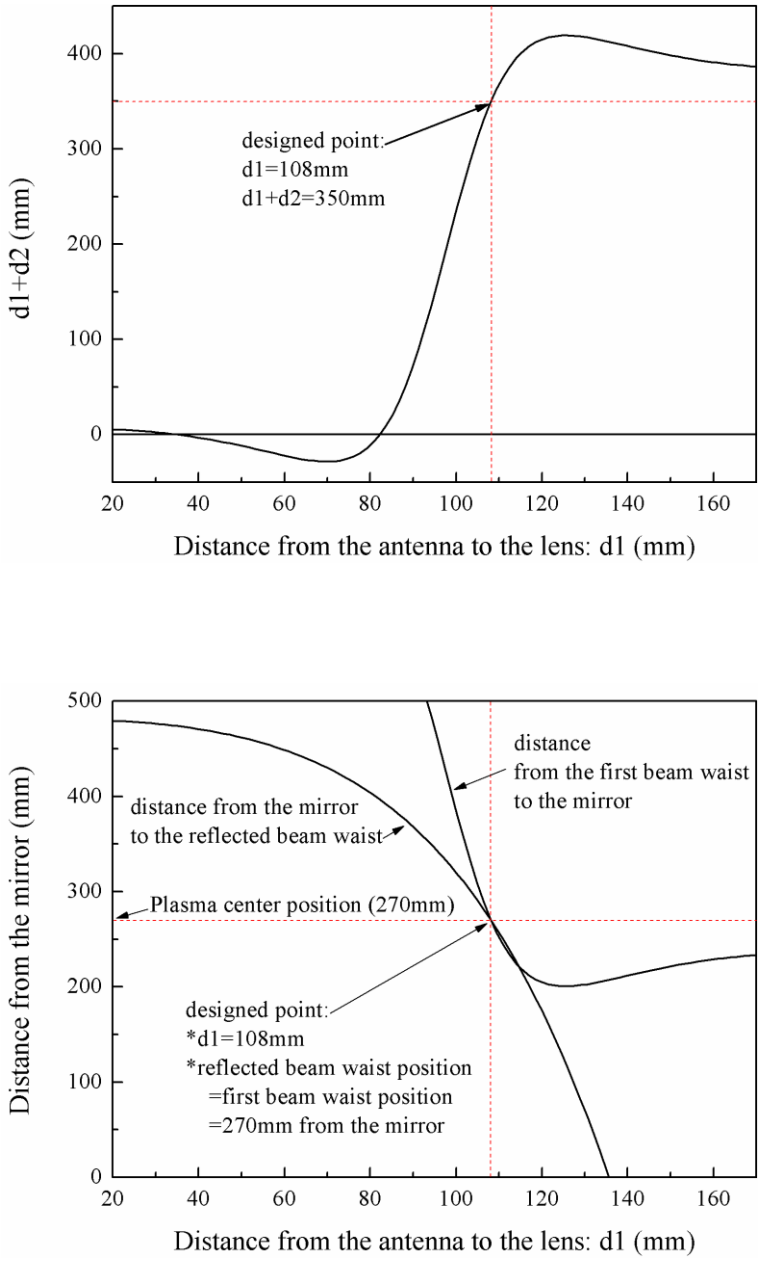

Figure 5.12 (up) Calculated results for relations between d1 and d1+d2 (down) Calculated results for relations between d1 and the distances from the mirror to each beam waist

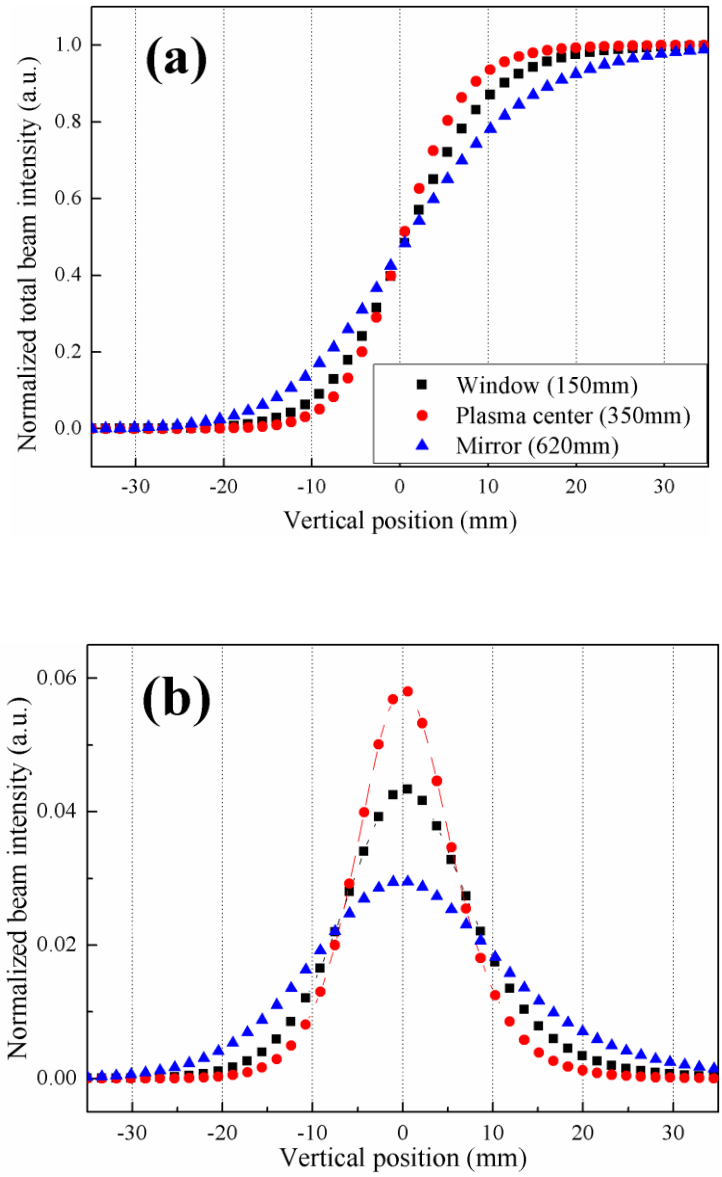

Figure 5.13 (a) Blocking plate is moved vertically downward in order to measure the total beam intensity at the position of window (black square, 150 mm from the antenna), plasma center (red circle, 350 mm from the antenna), and mirror (blue triangle, 620 mm from the antenna). (b) The beam intensity profile transverse to the beam path was obtained from the derivative of the total beam intensity.

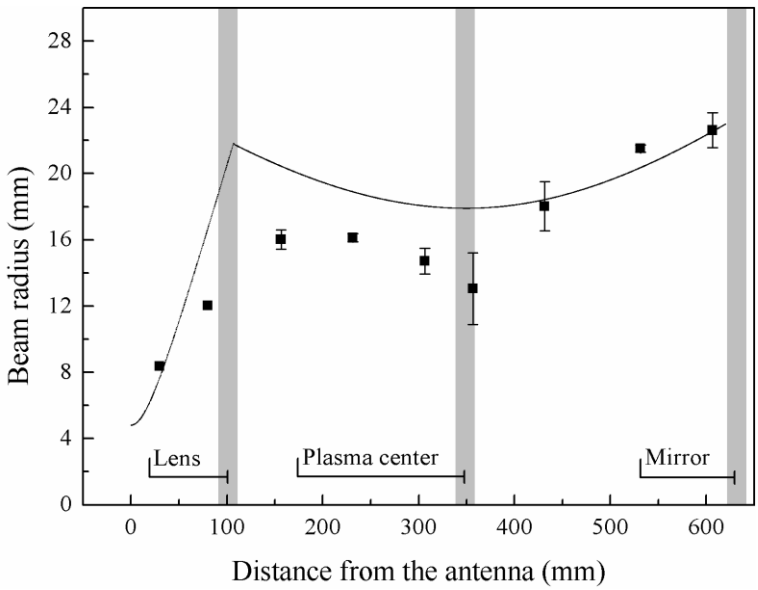

Figure 5.14 The beam radius (square dot) from the experiments had its lowest value near the plasma center position and overall values showed a similar tendency in agreement with the calculated beam radius.

Chapter 6 Test experiments on VEST

6.1 Installation on VEST

6.1.1 Overall features

Fabricated interferometer system with single chord configuration of horizontal plane has been installed in front of square port (3UR) at the upper chamber. Square port uses quartz window of thickness 15 mm and its width is about 120 mm, large enough for designed beam focusing system. Inner reflecting mirror is installed to the position of vertical plasma center in the upper chamber.

Figure 6.1 shows installed photo, in which circle corresponds the interferometer system including both microwave electronics system and beam focusing system. Small photo in the left-hand corner shows horn antennas and beam focusing systems, in which two Teflon lenses and inner reflecting mirror have been installed.

In addition to the setting in Figure 6.1, square quartz window is covered with mesh of 10 mm square grid, in order to prevent the effect of 2.45 GHz ECH microwave on electronic components.

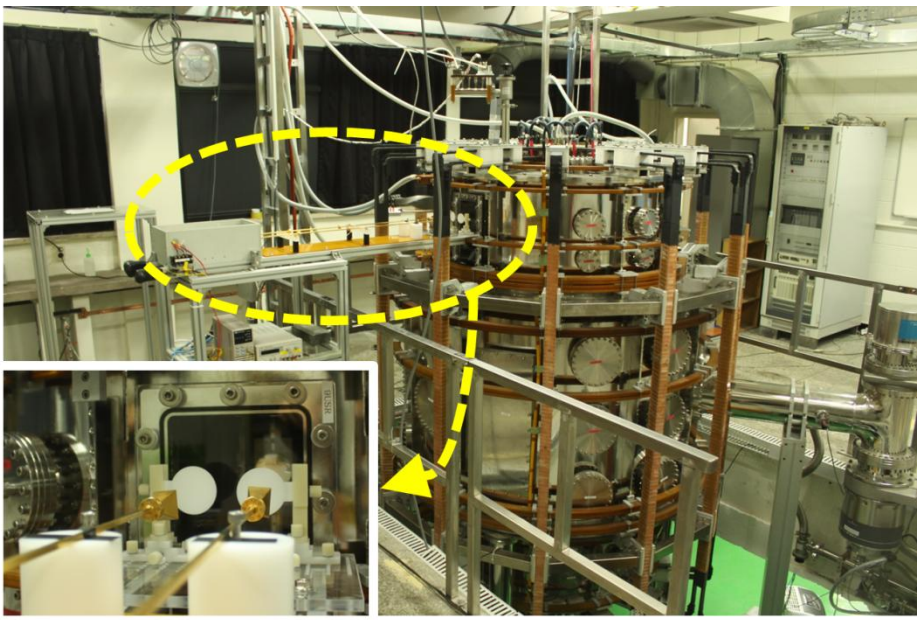

Figure 6.1 Interferometer system of horizontal plane configuration has been installed at the upper chamber. Circle in the photo indicates interferometer system and small photo in the left-hand corner shows beam focusing system, which comprises Teflon lenses and inner reflecting mirror.

6.1.2 Components testing

After the installation on VEST, component tests have been done to optimize alignment of optical components for beam focusing and to verify its ability on phase shift measurement. As did in the previous chapter, lens position optimizing test has been done moving lenses between horn antennas and window. Since total beam intensity is proportional to the amplitude of receiving beam, this amplitude is read at oscilloscope for various lens positions. Corresponding results are shown in Figure 6.2 as previously obtained Figure 5.11. Optimum position for lenses (94 mm) is slightly differ from the optimum position previouly obtained from test (91 mm) outside of the VEST. Although previous experiments copied the real VEST geometry, since that test system does not include quartz window, this deviation is expected to the effect of quartz window. However, this result shows very good agreement with the previous result, thus it can be seen that the interferometer system is well installed.

In order to obtain line integrated plasma density, phase difference is measured from interferometer system. The ability of this interferometer system to measure phase difference is verified by measuring phase difference of quartz plate of which refractive index is known as 2.1063 [11]. Two quartz plate of 10 mm and 20 mm are located in front of horn antennas, thus both launching and receiving beam transmitted quartz plate. Therefore corresponding path length becomes 20 mm and 40mm. Phase shift results are shown in Figure 6.3 in fringe number. Solid line and dash line both corresponds to calculated phase shift with given refractive index of quartz for 20 mm and 40 mm. Since calculated results excess above 1 fringe, calculated results are shifted to represent phase shift within 1 fringe. Measured phase shift fringe number corresponds two points in Figure 6.3, which lie in calculated phase shift line in a good agreement. Therefore, measurement of phase shift by this interferometer is reliable to measure line integrated plasma density.

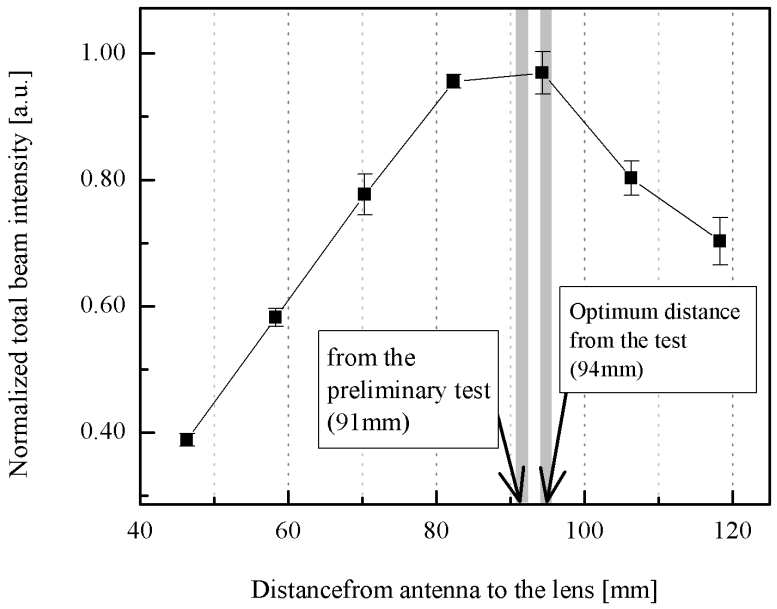

Figure 6.2 Beam focusing system test for optimize lens alignment**.**

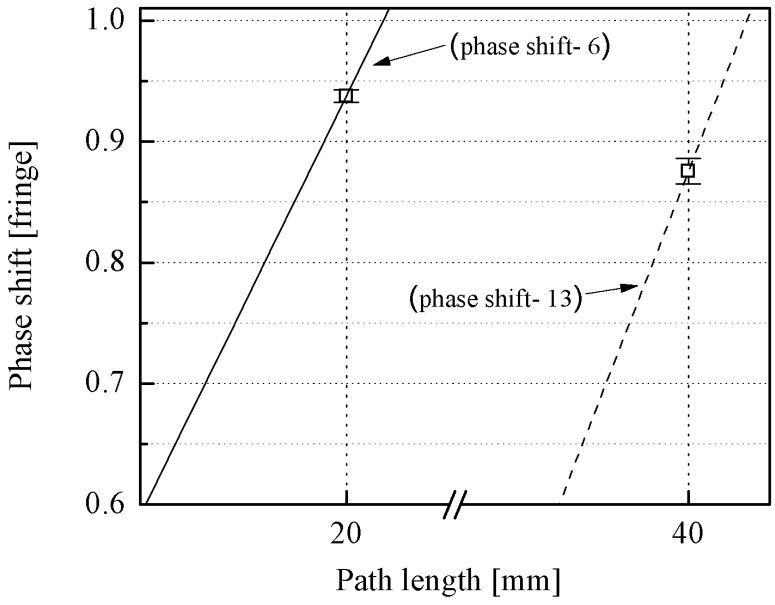

Figure 6.3 Phase shift measurements with quartz of known refractive index with different thicknesses show good agreement with estimated value by calculation

6.2 Test on ECH pre-ionization experiment

In the previous section, the interferometer system was installed on VEST and component test results showed that beam focusing system and phase shift measurement are reliable. In this section, the interferometer measures phase shift on electron cyclotron heating (ECH) pre-ionization experiment in order to verify its performance comparing its result with the triple probe measurement result.

6.2.1 Experimental setup

For the initial phase of operation in the VEST, double null merging startup experiments are planned, which two plasmas generated by partial solenoid coils at upper and lower chambers merge to make plasma current in the main chamber. In this start-up phase, ECH pre-ionization is necessary to provide low loop-voltage start up with limited volt-seconds [25, 26]. Two 2.45 GHz microwave injection systems utilizing cost-effective homemade magnetron power supplies of 3 kW power each have been designed and fabricated, and one is installed on port 7US6 at the upper chamber, as shown in Figure 6.4.

In order to find optimum matching condition for the ECH launcher, a series of experiments have been done changing matching conditions at three-stub tuner. Except for changing matching conditions, other operating conditions are kept unchanged: immediately after TF current reaches the flat-top at 100 ms, the ECH pre-ionization power is turned on. PF current was turned off during these experiments and base pressure and operation pressure was each 1.5E-6 torr and 3.2E-6 torr with helium gas of 0.6 sccm.

In order to measure electron density and temperature in a series of these

experiments, Langmuir triple probe has been used [2, 6, 7]. Langmuir triple probe enables high spatial resolution density measurements and electron temperature measurements without producing a full I-V sweep. It comprises three separately biased cylindrical collectors, and those checks three separate points on the plasma I-V curve at the same time, which allows high temporal resolution [6]. Triple probe is installed at port 4US6, next to the port of interferometer, 3UR. Its vertical location is same as horizontal plane of the interferometer, where probing beams are placed, while probe tip location is fixed at R=40 mm.

Phase shift signal from microwave electronics system of the interferometer is measured through oscilloscope at a particular time by external trigger signal. Two kinds of experiments have been done. One compares interferometer measurement results with triple probe measurement to verify whether interferometer results are reliable or not. Since triple probe measurement provides electron density at a particular location, while interferometer provides line integrated density, optical path length also could be determined.

The other experiment compares line integrated density of interferometer at two different times in one shot by triggering two times. In other words, in a series of shots of #1177 and #1179, ECH triggering signal was sent at 1100 ms. In a series of these experiments, ECH matching conditions are changed thus measured value are changed at each shots since matching condition changes plasma condition. However, because this interferometer measurements aim for verifying its performance only, no further analysis about matching conditions will be addressed.

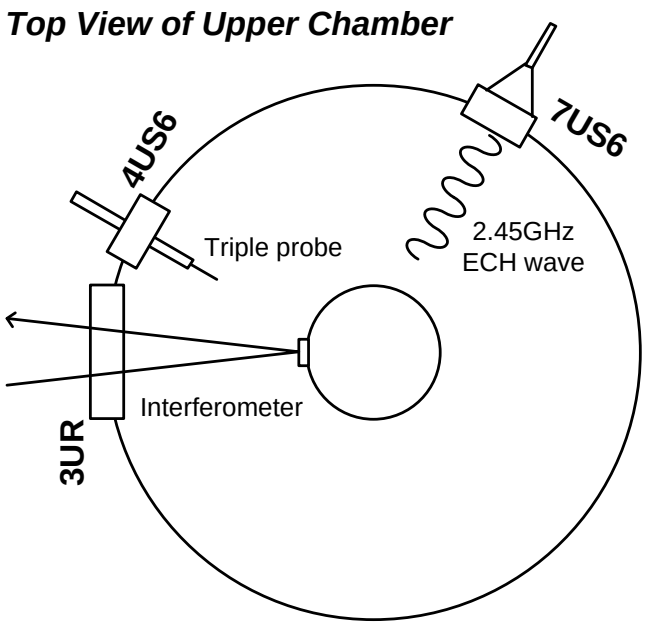

Figure 6.4 Top view of ECH X-mode launcher for pre-ionization (port 7US6), triple probe (port 4US6) and interferometer (port 3UR) installed at the upper chamber

6.2.2 Experimental results and discussion

Prior to discuss on experimental results, comparison method between triple probe and interferometer measurements needs to be addressed. Interferometer measures phase shift, which are proportional to line integrated density through its optical path, while triple probe provides plasma density per volume. Therefore, phase shift is proportional to both plasma density and optical path length. In other words, even if phase shifts give identical value with regard to different measurements, it cannot be ensured that two measurements have the same plasma property. These situations are represented in Figure 6.5, that for the same phase shift value, plasma density of 500 mm path length is lower than that of 200 mm path length. Uniform plasma profile has been assumed.

In Figure 6.6, the interferometer measurement results are plotted with the triple probe measurement results. With an assumption that plasma density profile is uniform, plasma density is deducerd from line integrated density for path length of 300 mm, 400 mm and 500 mm. In other words, uniform plasma density is assumed to be placed along the beam path by 300 mm, 400 mm and 500 mm. From this result, if the plasma profile is assumed to be uniform and triple probe measurement is reliable, then the plasma could be considered to be diffused throughout the horizontal plane, about 500 mm. In addition, in order to estimate electron density more precisely from line integrated density, more additional calibration process for electron density is needed.

However, the most important thing from this result is that regardless of the beam path length, overall density tendency and density range are similar to both measurement results. Measured electron density is expected to range from $4\times10^{16}m^{-3}$ to $9\times10^{16}m^{-3}$ with assumption of uniform profile and path lengths from 300 mm to 500 mm, which is almost similar to the result of triple probe, which ranges from $3\times10^{16}m^{-3}$ to $6\times10^{16}m^{-3}$. Therefore, this interferometer could reliably measure line integrated electron density.

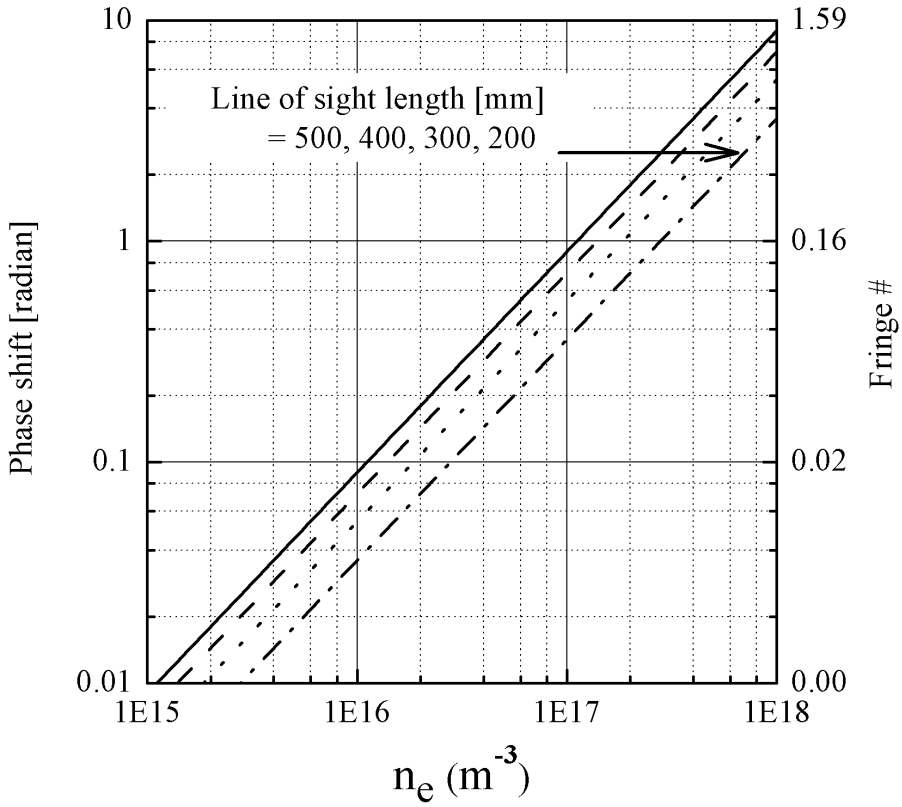

Figure 6.5 Plasma density estimation from phase shift value with different line of sight length.

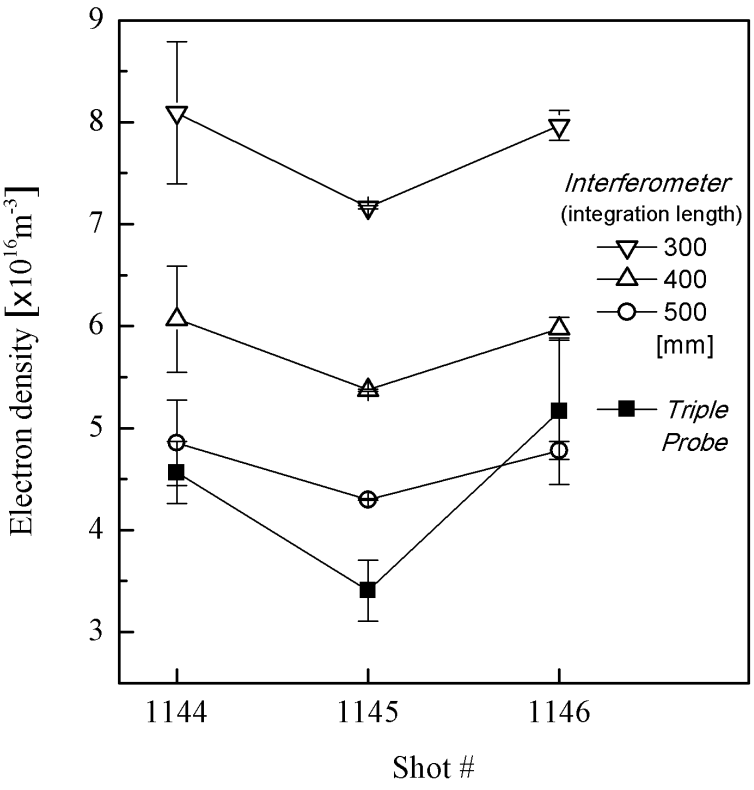

Figure 6.6 Electron density measurements results from triple probe are compared to the interferometer results which have been analyzed for different integration length.

Chapter 7 Conclusions and future work

7.1 Summary

The work presented in this thesis deals with developing of interferometer system for the VEST, which comprises 94 GHz heterodyne microwave system and beam focusing system. The major task of this research was analyzing constraints of the VEST, design overall interferometer system including microwave electronics system and beam focusing system and test developed system to verify its ability to measure plasma electron density. Specific works have been done at each task is summarized below:

Design of overall interferometer system for the VEST

For the VEST device, double-path interferometer system which utilizes inner mirror as reflecting material is designed considering its geometrical effect on refraction. The single chord measurement configuration of which both beams of double-path are lie in horizontal plane, can measure several shots by moving vertically in repeating identical shots. This measurement is simple and economical to apply. However, due to low aspect ratio of the device, size of inner reflecting mirror is restricted. Therefore beam focusing system is needed for the interferometer to enhance its spatial resolution and also place its beam waist at plasma center to measure phase shift more effectively. The beam focusing system configuration with the plano-convex lenses was chosen for the VEST interferometer, where a large volume for the focusing system is not available.

Optimizing microwave electronics system

Selecting optimum frequency for microwave electronics system required to satisfy low frequency limits and high frequency limits. There are three low frequency limits: frequency should be higher than the cutoff frequency of 28 GHz, wavelength should be lower than 4 mm (frequency higher than 75 GHz) to minimize deflection, and with regard to fringe jump, waves in millimeter range is apt to be utilized. And there are two high frequency limits exist, one is beam path change due to vibration and the other is resolution of density measurement. With regard to both limits, waves in millimeter range were found to be applicable. Therefore, among available microwave sources, 94 GHz wave was selected for the VEST interferometer system at initial operation phase. Two 94 GHz Gunn oscillators with a frequency difference of 60 MHz is used in the microwave electronics part of a heterodyne interferometer system of Mach-Zehnder configuration.

Design of beam focusing system depending on measurement configurations

Beam focusing system aims at maximizing the effective beam reception and spatial resolution. Depending on quasi-optics theory, optical elements were designed for two possible measurement configurations discussed in chapter 2. At first, system requirements were discussed for the VEST system, and optimum specification of Teflon lens and stainless steel mirror with their relative distances were analyzed. For single chord measurement system, lens of 43mm radius and concave mirror of 270 mm was chosen in order to place beam waist at plasma center. For vertical scanning measurement system, beam focusing systems were designed separately on E-plane and H-plane. For E-plane, lens of 85mm radius was chosen to locate beam waist at plasma center as designed for single chord measurement configuration. For H-plane, lens of 115mm radius was chosen to locate beam waist at the mirror since mirror cannot focus in vertical plane. Simulation results show that the spatial resolution is enhanced with the beam focusing system higher than 10 times than that without focusing system.

Testing the developed system to verify its ability to measure plasma electron density

The design of the beam focusing system and beam path analysis were verified with a couple of experiments done within an experimental framework that considered the real size of a vacuum vessel. Since the single chord measurement configuration will be used at the initial phase of operation, this configuration was used to find optimum distance between horn antenna and lens, of which result shows good agreement with designed specifications. In addition, using knife-edge method, beam radius was measured for several positions, and result agreed well with the predicted result by calculation and also showed the spatial resolution with beam focusing system is 6 times better than that without beam focusing system

After then, test experiments on VEST were done in order to verify the designed system which is installed at upper chamber. Test experiment was used to optimize the system and verify its ability to generate phase shift signal using quartz of known refractive index. Also, measurements on ECH pre-ionization experiments had been done. With an assumption of uniform density profile, electron density variation tendency over shots showed overall agreement with the results from triple probe measurement. Also, measured electron density was expected to 4E16~9E16 m^{-3} with assumption of uniform profile and path lengths of 300~500 mm, which is almost similar to the result of triple probe, 3E16~6E16 m^{-3}. However, additional information is needed in order to precisely deduce plasma electron density from the line-integrated density.

7.2 Conclusions and future work

From the test results of developed interferometer system on ECH pre-ionization experiment that electron density measurement results show similar tendency and lie in the same range with triple probe measurement results, the interferometer system developed in this thesis is reliable to be employed.

This work optimized the interferometer system for the VEST device, low aspect ratio spherical torus. Designed beam focusing system enhanced the spatial resolution significantly, but this kind of beam focusing system design process has not been tried yet. Therefore design methods used in this thesis are expected to be applied to other devices, not only for the fusion plasma device, but also low temperature plasma devices.

In addition, although only single chord measurements have been done in this thesis, designed vertical moving measurement configuration will be fabricated in a near future and vertical distribution of line integrated density will be measured. It will be operated by linear guide installed on overall interferometer system. And using appropriate inversion technique, plasma density profile is expected to be determined.

Appendix A
Single chord measurement on vertical plane

A.1 Plasma density profile estimation methods

Although interferometer provides reliable information on plasma electron density, it only measures line integrated plasma electron density along beam path. If the plasma density profile can be seen as uniform along the beam path, then line integrated plasma electron density itself could represent average plasma electron density. However, for many cases plasma density profile has non uniform profile, rather parabolic profile, thus plasma density profile estimation is necessary for further understanding of the plasma.

One of the best-known estimation method is Abel inversion, which deduces the radial distribution from the multi-channel line integral measurements using the known mathematical properties of the Abel transform [2, 27]. This can be applied when plasmas have the property of cylindrically symmetric.

If we assume that cylindrically symmetric quantity as *f(r)*, then the line integrated quantity from measurements would be,

$$F(y)=\int_{-\sqrt{(a^2-y^2)}}^{+\sqrt{(a^2-y^2)}} f(r)dx = 2\int_y^a f(r)\frac{rdr}{(r^2-y^2)^{1/2}} \qquad \text{(A.1)}$$

where radius is *a* and radial variable is *r* and $x^2+y^2=r^2$. The inverse transform relates *f(r)* to an integral of *F(y)* the measured quantity at line of sight,

$$f(r)=\frac{1}{\pi}\int_a^r \frac{dF}{dy}\frac{dy}{(y^2-r^2)^{1/2}} \qquad \text{(A.2)}$$

provided that $f(a)=0$. Thus line integrated density measurement enable to deduce original cylindrically symmetric quantity, plasma density.

The other method from single chord measurement use vertical movement of plasma and restricted for special interferometer configuration, a triangular beam path which does not pass through the plasma axis in KSTAR device [28, 29]. With the position data of plasma and an estimated plasma profile, the peak density and the mean density could be obtained from the line integrated density. The measured line integrated densities of the plasma at different positions due to the vertical motion provide an opportunity to estimate the local electron density. Especially for the KSTAR last operation, plasma shape could be assumed as circular, thus in this plasma profile could be deduced with the position and the size of the plasma obtained from an analysis of television image. The estimation result with the model for the scrape-off region showed that parabolic density profile is reasonable when the plasma is placed at the center of tokamak. Although it needs additional information on plasma property, this deduction procedure has merits in simple configuration.

In conclusion, both methods could be utilized to deduce plasma density profile from measured line integrated density value. Although Abel inversion is based on multi-chord measurement, single chord measurements vertically moved between shots can also apply the inversion method, with an assumption of constant plasma conditions. If then, by just changing configurations, single chord measurement could be applied to both density profile estimation method.

A.2 Single chord measurement

Two of single chord measurements plans use horizontal plane and vertical plane configuration, as shown in Figure A.1. As discussed in the previous chapter, vertical plane configuration could be used to verify vertically moving plasma. Similar study had been done [29] about moving plasma at the end of the discharge. Electron density profile was determined with assumptions of profile shape and geometry of plasma based on camera images. In the VEST plasma, plasma moves down at the upper chamber in plasma merging start up phase, thus similar analysis could be applied if appropriate method for determining vertical movement is provided by such as camera images.

With the aid of phase comparator, line integrated plasma density evolution could be measured. From the line integrated plasma density results with time, electron density profile information could be determined with assumptions of plasma shape and vertical movement information. As opposed to this procedures, prior to the experiments, with an assumption that plasma moves at constant speed with a certain profile, expected line integrated plasma density is determined from simulation.

For a simplified system, plasma electron density is assumed as to have a circular shape and has a parabolic profile as

$$n_e(r) = n_0\left(1-(r/a)^2\right)^b \tag{0.2}$$

where n_0 is peak density, a is plasma minor radius and b is parabolic parameter. Plasma density profiles are estimated for several cases changing the value of b from 0 to 2, and minor radius is 0.3m and major radius is 0.4m. These estimated density profiles are represented in Figure A.2. Vertical position of horizontal axis in the Figure corresponds to position at circular plasma from outside to opposite outside via center.

Simulation results are shown in Figure A.3 for different plasma density

profiles determined from Figure A.2. Circularly shaped plasma is moved at constant speed; time of zero corresponds the time when plasma touches upper probing beam for the first time. As plasma moves down, broader portion of probing beam encounters the plasma, thus line integrated density increases. Before the line integrated density reaches the maximum value, there is a discontinuous point of its derivative, at which circular plasma starts to encounter lower probing beam. And the other discontinuous point of its derivative, after the maximum point, corresponds to the case when circular plasma comes out from the upper probing beam.

Since all circular plasma have same radius and same speed in the simulation, ending time and overall shape is same for all cases. However, as *b* increases plasma profile becomes narrow, thus line integrated density value decreases at the same point.

These results are expected to be measured when moving plasma condition satisfies constant speed and circular shape. If then, similar plasma profile could be determined from these results. Even if these results are restricted for very ideal case with some assumptions, these give an idea to deduce plasma profile with the aid of information on vertical movement

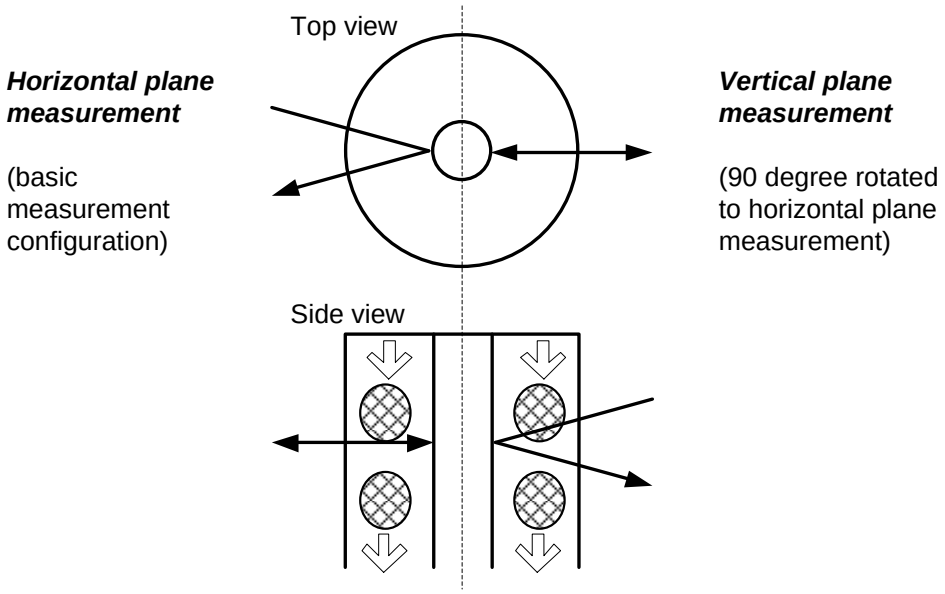

Figure A.1 Single chord measurements configurations of vertical plane measurement and horizontal plane measurement

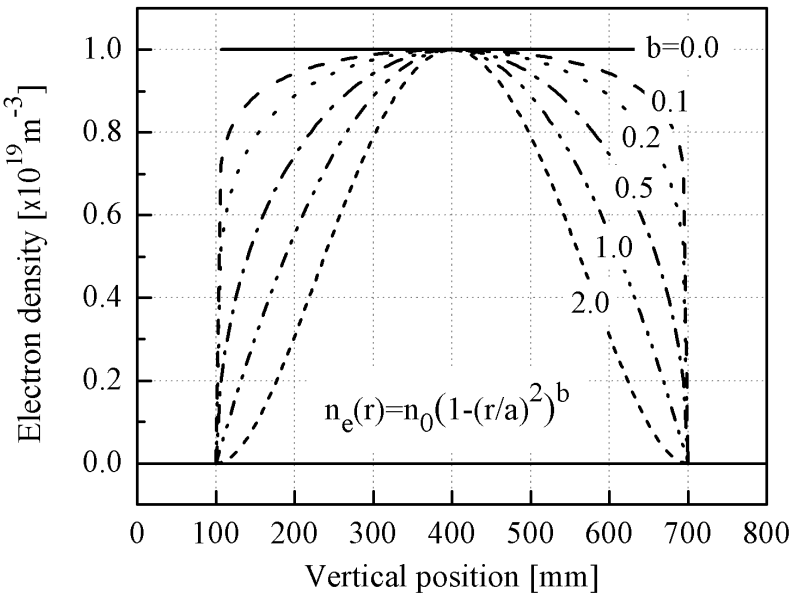

Figure A.2 Various parabolic density profiles which are used for simulations

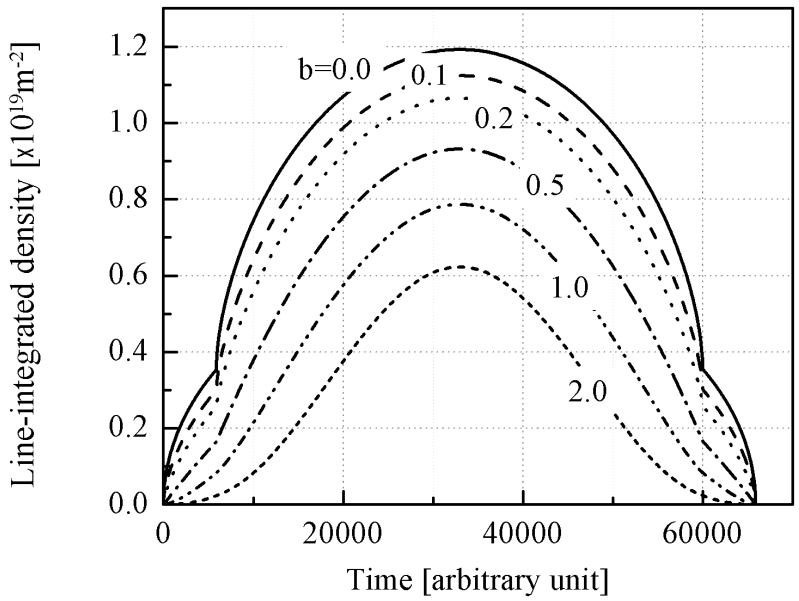

Figure A.3 Simulation results for line integrated density, which is expected to be measured in the measurement with the aid of phase comparator. Circularly shaped plasma with density profiles in Figure A.2 is used and moved constantly downward.

A.3 Vertical moving measurement

As shown in Figure A.1, vertical scanning measurement uses horizontal plane configuration and measure line integrated density at different vertical position at different each shot. All experimental conditions remain unchanged, but only vertical measuring position could move with the aid of the linear guide. Through these measurements, line integrated density at each vertical position could be obtained, and if circular shape of plasma with a profile of cylindrical symmetry is assumed, then plasma profile could be deduced from Abel inversion as discussed in section A.1.

On the contrary to this inversion method, if we use several plasma density profiles presented in the previous section, expected line-integrated density can be obtained from simulation. Figure A.4 shows the result; x axis represent vertical scanning position from plasma center. Therefore, line integrated density decreases because density profile decreases radially and also beam path length in the plasma decreases. Also, at the same vertical scanning position, plasma with narrow profile shows lower line integrated density. These results could be also predicted from Figure A.2, since each line averaged density at vertical position corresponds to area from center to the vertical position. In real vertical scanning measurement, plasma profile shape can be predicted from this simulation result.

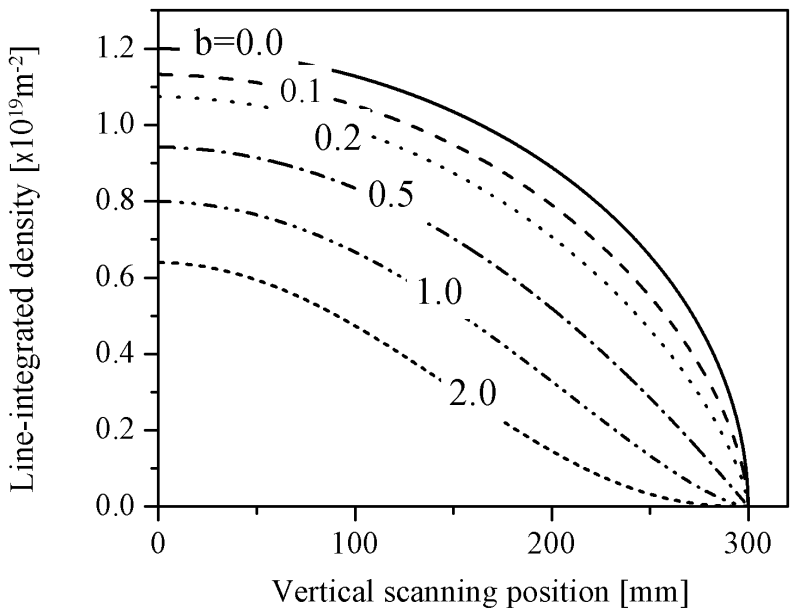

Figure A.4 Expected line integrated density for various plasma profiles from vertical scanning measurement. Vertical scanning position corresponds to the distance from center of central plasma, of which radius is 300 mm.

Abstract (in Korean)

초 록

VEST 장치를 위한 간섭계 시스템 개발

최다혜

에너지시스템공학부

서울대학교 대학원

서울대학교 다목적 실험용 구형 토러스 (VEST) 장치의 플라즈마 밀도를 측정하기 위한 마이크로파 간섭계 시스템이 개발되었다. VEST의 초기 운전은 주로 중심축의 수직 끝에 설치된 두개의 부분 솔레노이드 코일을 이용한 double null merging 스타트업을 중심으로 하게 된다. 밀도 분포의 변화는 이 장치의 플라즈마 특성을 알기 위해 진단되어야 할 중요한 특성이다. 본 간섭계 시스템은 수평면의 선적분된 플라즈마 밀도를 각각의 동일한 조건의 운전마다 수직으로 움직이면서 측정하도록 설계되었고, 94 GHz 주파수의 마흐 젠더 타입의 헤테로다인 단채널 간섭계와 빔 포커싱 시스템이 실제로 설치되었으며 테스트가 이루어졌다.

본 간섭계 시스템은 94 GHz 헤테로다인 마이크로파 시스템과 빔 포커싱 시스템으로 구성되어 있다. 94 GHz의 주파수는 컷오프 주파수, 측정 밀도의 분해능, 진동 및 굴절에 의한 영향을 고려하여 결정되었다. 이 마이크로파 시스템은 마이크로파를 입사하고 위상

이 변화된 빔을 수신하여 전기 회로 상에서 플라즈마 밀도를 측정할 수 있는 신호를 생성한다. IF 주파수는 60 MHz 정도로 설정되었으며, 두 개의 믹서에서 나오는 신호의 위상차는 위상 비교회로에 전송되어 위상차에 비례하는 전압 신호를 생성하게 된다.

또한 준광학계 가우시안 빔 경로 분석에 따라, 빔의 초점을 맞추고 반사를 가능하게 하여 효율적인 빔 수신 및 공간 분해능을 증가시키는 빔 포커싱 시스템이 설계되었다. 단채널 시스템의 경우 평면-곡면의 구형 렌즈 한 쌍과 오목의 원형 거울로 설계되었다. 그리고 수직 스캔 측정의 경우 두 쌍의 평면-곡면의 실린더형 렌즈 두 쌍과 오목의 실린더형 거울로 구성하여 설계되었다.

이어서 단채널 시스템 측정을 위해 설계된 빔 포커싱 시스템과 빔 경로 분석이 실제 진공 용기와 같은 크기를 갖는 실험 조건에서 실험적으로 확인되었다. 광학 부품들 사이의 최적 거리와 빔 경로를 따른 빔 반경 측정 결과는 가우시안 광학에 따라 분석된 결과와 잘 일치한다. 실험과 수치적 계산 결과를 통해 설계된 빔 포커싱 시스템이 시스템의 공간 분해능을 20 mm 이상으로 높이게 되며, 또한 최소 빔 반경 지점이 플라즈마 중심에 위치하게 되어 플라즈마에서의 위상 변화를 더욱 효과적으로 생성할 수 있다.

이러한 실험에 기초하여, 수평면의 단채널 구조가 VEST의 상부 용기에 설치되었다. 구성 부품 테스트를 통해 빔 포커싱 시스템 정렬이 최적화 되었으며 굴절률이 알려진 물질을 통해 위상 변화를 시험해 본 결과 이론적으로 예측되는 값과 일치하는 것을 확인했다. 또한, ECH 전이온화 실험에 대한 측정이 이루어졌으며, 그 결과 값이 트리플 프로브의 측정 결과 값과 비교되었다. 플라즈마 전자 밀도가 측정된 선적분된 밀도 값에서 추정되었으며, 그 값은 트리플 프로브의 결과와 거의 일치함을 보였다. 이 논문에서 개발된 단채널 간섭계 시스템은 VEST의 스타트업 단계에서 플라즈마의 선적분된

밀도값을 측정하는 데에 쓰일 것이며, 근 시일 내에 수직 스캐닝이 가능한 완전한 간섭계 시스템의 제작이 완료되어 플라즈마 밀도 분포 측정을 가능하게 할 것이다.

주요어 : 간섭계, VEST, 플라즈마 전자 밀도 진단, 밀리미터파 웨이브, 가우시안 빔, 준광학계 시스템

학번 : 2010-23347

Biblography

1. Donné, A., et al., *Diagnostics.* Nuclear fusion, 2007. 47: p. S337.
2. Hutchinson, I.H., *Principles of plasma diagnostics*2005: Cambridge Univ Pr.
3. Petrov, A. and V. Petrov, *Time-of-flight refractometry for robust line integral electron density measurements and control in ITER.* Review of Scientific Instruments, 2003. 74: p. 1465.
4. Kawano, Y., S. Chiba, and A. Inoue, *Infrared laser polarimetry for electron density measurement in tokamak plasmas.* Review of Scientific Instruments, 2001. 72: p. 1068.
5. Park, H., et al., *Far infrared tangential interferometry/polarimetry on the National Spherical Tokamak Experiment.* Review of Scientific Instruments, 1999. 70: p. 710.
6. Deline, C., et al., *High accuracy plasma density measurement using hybrid Langmuir probe and microwave interferometer method.* Review of Scientific Instruments, 2007. 78(11): p. 113504-113504-7.
7. Neumann, G., et al., *Plasma-density measurements by microwave interferometry and Langmuir probes in an rf discharge*. Review of Scientific Instruments, 1993. 64(1): p. 19-25.
8. Chen, F.F., *Introduction to plasma physics and controlled fusion: plasma physics*. Vol. 1. 1984: Springer.
9. Button, K.J., *Infrared and millimeter waves. Volume 2-Instrumentation.* New York, Academic Press, Inc., 1979. 373 p (For individual items see A80-34969 to A80-34973), 1979. 1.
10. K. J. Chung, Y.H.A., B. K Jung, H. Y. Lee, C. Sung, Y. S. Na, T. S. Hahm and Y. S. Hwang, *Design Features and Commissioning of Versatile Experiment Spherical Torus (VEST) at Seoul National University.* Plasma Science and Technology, To be published.
11. Goldsmith, P.F., et al., *Quasioptical systems*1998: Chapman & Hall.

12. Efthimion, P., et al., *1-millimeter wave interferometer for the measurement of line integral electron density on TFTR.* Review of Scientific Instruments, 1985. 56(5): p. 908-910.
13. Fessey, J., et al., *Plasma electron density measurements from the JET 2 mm wave interferometer.* Journal of Physics E: Scientific Instruments, 1987. 20: p. 169.
14. Forest, C., G. Greene, and M. Ono, *CDX-U two-dimensional scanning microwave system.* Review of Scientific Instruments, 1990. 61(10): p. 2888-2890.
15. Nam, Y., et al., *Design of a single-channel millimeter-wave interferometer system for Korea Superconducting Tokamak Advanced Research.* Review of Scientific Instruments, 2003. 74: p. 1613.
16. Nam, Y. and K. Lee, *A 280; GHz single-channel millimeter-wave interferometer system for KSTAR.* Review of Scientific Instruments, 2008. 79(10): p. 10E705-10E705-3.
17. Chang, e.b.K., *Optical components*. Handbook of microwave and optical components ; v. 3, ed. K. Chang. Vol. 3. 1990, New York: J. Wiley.
18. Chang, e.b.K., *Microwave passive and antenna components*. Handbook of microwave and optical components ; v. 1. Vol. 1. 1989, New York: J. Wiley.
19. Malacara, D. and Z. Malacara, *Handbook of optical design*. Vol. 85. 2004: CRC.
20. Self, S.A., *Focusing of spherical Gaussian beams.* Applied Optics, 1983. 22(5): p. 658-661.
21. Greenwald, M., *Density limits in toroidal plasmas.* Plasma physics and controlled fusion, 2002. 44: p. R27.
22. Chung, J., et al., *Descriptions of a linear device developed for research on advanced plasma imaging and dynamics.* Review of Scientific Instruments, 2009. 80: p. 103503.
23. Devarapalli, N., et al., *Design and implementation of a 120 GHz tracking interferometer with near diffraction limited focal spot.*

Review of Scientific Instruments, 2008. 79: p. 093509.

24. Suzaki, Y. and A. Tachibana, *Measurement of the μm sized radius of Gaussian laser beam using the scanning knife-edge.* Applied Optics, 1975. 14(12): p. 2809-2810.

25. Lloyd, B., et al., *Low voltage ohmic and electron cyclotron heating assisted startup in DIII-D.* Nuclear fusion, 1991. 31: p. 2031.

26. Holly, D., et al., *Tokamak start-up with electron-cyclotron heating.* Nuclear fusion, 1981. 21: p. 1483.

27. Vest, C., *Interferometry of strongly refracting axisymmetric phase objects.* Applied Optics, 1975. 14(7): p. 1601-1606.

28. Nam, Y. and J. Chung, *Analysis of line integrated electron density using plasma position data on Korea Superconducting Tokamak Advanced Research.* Review of Scientific Instruments, 2010. 81: p. 10D510.

29. Kim, M., et al. *Deduction of electron density profile information from a single chord interferometry on KSTAR*. 2009. IEEE.